FISEVIER

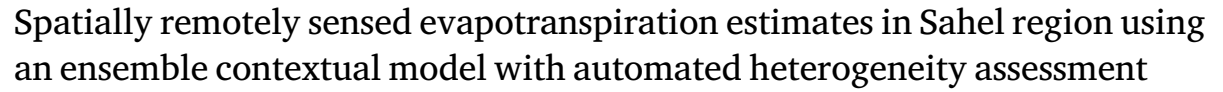
Contents lists available at ScienceDirect

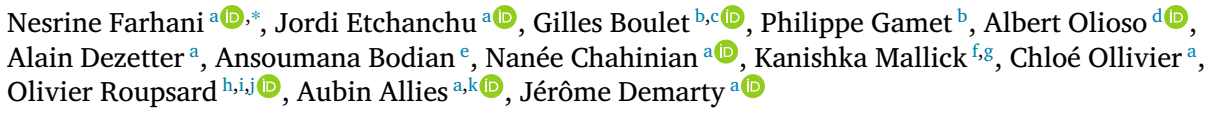
Science of Remote Sensing

journal homepage: www.sciencedirect.com/journal/science-of-remote-sensing



Full length article





- ^a HydroSciences Montpellier (HSM), Univ Montpellier, CNRS, IRD, 15 Av. Charles Flahault, 34093 Montpellier, France
- b Centre d'Etude Spatiales de la Biosphere (CESBIO), Universite de Toulouse, CNRS, CNES, IRD, UT3, INRAE, Toulouse, France
- c Indo-French Cell for Water Science, ICWaR, Indian Institute of Science, Bangalore, India
- ^d Unite de Recherche ecologie des Foret Mediterraneennes (URFM), INRAE, 84000 Avignon, France
- ^e Laboratoire Leidi Dynamique des Territoires et Developpement, Universite Gaston Berger (UGB), Saint Louis, Senegal
- f Department of Environment Research and Innovation, Luxembourg Institute of Science and Technology, Belvaux 4362, Luxembourg
- E Department of Environmental Science, Policy, and Management, University of California, Berkeley, CA 94720, United States
- h Eco Sols, Univ Montpellier, CIRAD, INRAE, IRD, Montpellier SupAgro, Montpellier, France
- i CIRAD, UMR Eco Sols, BP1386, CP18524, Dakar, Senegal
- ¹ LMI IESOL, Centre IRD-ISRA de Bel Air, BP1386, CP18524, Dakar, Senegal
- k GreenTriangle SAS, 10 Rue De La Bourse, 75002, Paris, France

ARTICLE INFO

Keywords: Semi-arid Evapotranspiration Contextual EVASPA S-SEBI Sahel

ABSTRACT

Water scarcity and the inter-annual variability of water resources in semi-arid areas are limiting factors for agricultural production. The characterization of plant water use, together with water stress, can help us to monitor the impact of drought on agrosystems and ecosystems, especially in the Sahel region. Indeed, this region is identified as a "hot spot" for climate change. In-situ measurements often are insufficient for accounting for spatial variability at large scales (> 100 km) due to the scarcity of gauge networks. To tackle this issue, remotely sensed evaporation is often used. In this study, estimates using thermal infrared and visible data from MODIS/TERRA and AQUA are used. Spatially distributed estimates of the daily actual evapotranspiration (ETd) are simulated using the EVASPA S-SEBI Sahel (E3S) ensemble contextual method over a mesoscale area (145x145 km) in central Senegal. E3S uses a set of different methods in order to identify the dry and wet edges of the surface temperature/albedo scatterplot and therefore estimate the evaporative fraction (EF). However, contextual approaches assume the simultaneous presence of sufficient fully wet and fully dry pixels within the same satellite image. This assumption of heterogeneity does not always hold, especially in the Sahel, which is characterized by the alternation of dry and wet seasons due to the monsoon-influenced climate. To tackle this issue, E3S uses different sets of methods depending on the season, based on local knowledge. The present study thus aims at generalizing the approach by proposing a new version of E3S called "E3S-V2". This latter allows an automatic detection of different heterogeneity conditions. Therefore, a sensitivity analysis examining the effect of using different EF estimation methods over different spatial coverages was performed. It made it possible to identify relevant normalized indicators to determine the heterogeneity level, as well as to discriminate among the most adapted EF determination methods for each situation. From this analysis, an automated procedure of method selection according to the heterogeneity conditions is proposed. A local-scale evaluation was performed using eddy-covariance measurements in the Senegal Groundnut Basin. A spatialized evaluation was also performed using GLEAM and ERA5-Land, which are proven reference ETd products over the area. "E3S-V2" simulations yield comparable performances with in-situ and reference products in our study

E-mail addresses: nesrine.farhani@umontpellier.fr (N. Farhani), jordi.etchanchu@umontpellier.fr (J. Etchanchu).

Corresponding author.

1. Introduction

In semi-arid areas, water scarcity and the inter-annual variability of water resources are critical for natural and anthropic ecosystems (Norton et al., 2016). Indeed, these areas are extremely vulnerable to climatic changes and the modification of rainfall regimes (Panthou et al., 2018), including longer dry periods and more intense rainfall events (Trenberth, 2011). Ongoing climate changes intensify the evaporative demand; this is linked to a continuous increase in temperatures, which could lead to more frequent periods of drought (Vogt et al., 2018) and impact the hydrological cycle drastically (Ragab and Prudhomme, 2002). In fact, in semi-arid areas, more than 80% of the annual available water is lost through evapotranspiration (Chehbouni et al., 2008). This constitutes a serious threat given the limited water supply in these regions. In addition, a growing population, irrigation and livestock rearing, among other things, are increasing water consumption and affecting water availability. Therefore, an important issue in these countries is to provide accurate estimates of surface water deficits in a spatially distributed manner for water planning and management.

As evapotranspiration (ET) is a key factor for scarce water resources management, its estimation is critical. Direct measurements of turbulent heat fluxes could be performed for an accurate ET estimation. However, measurements are not able to account for the spatial variability of this variable in some regions, e.g., less developed countries, that are scarcely gauged. The growing number of spatial ET products offer an interesting alternative for addressing these issues. These products are generated using a wide range of methods, including empirical equations (e.g., the FAO56 method for the separate estimation of soil evaporation and crop transpiration, neural network approaches or data fusion), land surface models (LSMs), energy balance models or interpolated in-situ measurements. In Etchanchu et al. (2025), a comparison of 20 available ET products in the Sahel was conducted at both the local scale, using in-situ measurements, and mesoscale (100 \times 100 km). The results revealed that, currently, there is no product that simultaneously combines a good spatio-temporal resolution (e.g., <1 km, <daily) and good performance. Energy balance models can be a useful tool because they allow spatial ET estimates at various spacetime resolutions. These methods rely mainly on solving the surface energy budgets (Anderson and Kustas, 2008), which are expressed as a function of the land surface temperature (LST) acquired from remote sensing (RS) data, making it possible to determine the latent heat flux (LE). The LST can thus be used as a signature of the partition of available energy toward higher sensible (dry conditions) or latent (wet conditions) heat flux values (Sheffield and Wood, 2012). RS data in the thermal infrared (TIR) domain (3-15 µm) are therefore particularly informative for assessing water availability and thus for adjusting water requirements (Boulet et al., 2007).

TIR-based methods can be divided into two families: contextual and single-pixel methods (Chirouze et al., 2014). Contextual methods include all approaches based on the thermal contrast (hot/dry and cold/wet pixels) using the synchronous information of several pixels of a given image in order to compute a relative estimation of the water stress level at the satellite overpass (Bastiaanssen et al., 1998; Allen et al., 2007; Carlson, 2007; Roerink et al., 2000). Single-pixel methods, on the other hand, mostly solve the surface energy budget for each pixel independently from the others (Lagouarde and Boulet, 2016). The latter are more adapted to uniform landscapes with homogeneous vegetation and surface water conditions. Moreover, they can be more adapted to the use of low-resolution data that could cover many individual plots with different land-use in the same pixel (Chirouze et al., 2014). Nevertheless, unlike contextual approaches, single-pixel methods (Boulet et al., 2015; Norman et al., 1995; Su, 2002) are more sensitive to absolute errors in surface temperature estimates. Indeed, contextual methods require less meteorological data as input, which reduces the number of uncertainty sources and facilitates operational applications.

Contextual methods such as the Simplified Surface Energy Balance Index (S-SEBI) (Roerink et al., 2000) or the LST-VI triangle model (Jiang and Islam, 1999) are widely used due to their simple mechanism, lower data input requirements and appropriate performance (Chirouze et al., 2014; Jiang and Islam, 2001; Tang and Li, 2017; Carlson and Petropoulos, 2019). These methods assume that the differences in the LST are induced only by the evaporative cooling effect, ranging between the dry (hottest pixel) and wet (coldest pixel) boundaries, where ET is assumed to be, respectively, null (unavailability of soil moisture) and at potential ET (Tang et al., 2010). Consequently, for each pixel, the evaporative fraction (EF) can be estimated relative to its position between these two boundaries (Tang et al., 2010; Carlson, 2007; Zhu et al., 2020). The applicability and accuracy of these methods is limited mainly by two aspects. First, this approach assumes the presence of a sufficient heterogeneity between dry and wet pixels within the same image at the time of acquisition (Lagouarde and Boulet, 2016). This can be problematic when the conditions are quite homogeneous, e.g., immediately after rain events or during a dry season (Tang et al., 2010). Second, this method depends significantly on the correct identification of the dry and wet edges in the LST-VI space (Zhu et al., 2020). Indeed, the definition of the limiting edges of the EF determines the magnitude and frequency distributions of EF estimates significantly (Long and Singh, 2013). Moreover, the inappropriate selection of these two boundaries can induce the consistent overestimation or underestimation of the EF, which leads to unrealistic ET estimation (Long and Singh, 2013). A correct determination of the true dry and wet edges is thus critical, as it remains the main source of uncertainty in these approaches (Olioso et al., 2015).

In general, model boundaries are defined empirically from the image information using linear regressions or theoretically using different energy balance models. The wet edge, for example, is not always easy to identify due to cloud pixels (Carlson et al., 1995), which can produce anomalously low values of temperature. In order to simplify the procedure, the wet edge is generally identified by using the lowest observed clear pixel surface temperature in the image scene (Jiang and Islam, 2001) or by directly using the air temperature (Zhang et al., 2008; Liang et al., 2011) or the surface temperature of a water body (Zhang et al., 2008) and/or a well-irrigated agricultural area (Carlson, 2007). For the dry edge, most methods use scatterplots to fit it, which can lead in many cases to errors. Indeed, in some regions, a triangular (or trapezoidal) shape does not form well, so the dry edge cannot be easily identified. Second, the temperature of the observed dry edge is generally lower than that of the true dry edge (Liang et al., 2011). Consequently, in some studies, such as Zhang et al. (2008) or Liang et al. (2011), the dry edge is identified using a surface energy balance method to define the true driest bare soil and the true driest full-cover vegetation. However, resolving the energy balance equation usually requires complex parameterization and additional meteorological measurements, which constrain the generalization of the method and its operational applications (Carlson, 2007; Tang et al., 2010; Zhu et al., 2020). A variety of empirical algorithms are proposed for contextual method users for dry edge identification. Jiang and Islam (2003) apply a correction parameter to re-scale the EF and account for different water stress conditions at the dry edge: from 0 on bare soil to 1 on full vegetation cover when root zone soil water is not stressed. This method provides satisfactory results when no water stress conditions in the root zone occur at the observed dry edge (Jiang and Islam, 2003). In other studies, such as Tang et al. (2010), it is considered that when using satellite remote sensors, the dry edge (high LST pixels) is easily identified compared to the wet edge in arid and semiarid regions. Therefore, in these regions, the observed dry edge from the satellite remote sensors can represent the true dry edge. The EF is then determined using a water stress correction parameter (Jiang and Islam, 2003). However, the surface temperatures at the observed wet edge may be higher than at the true wet edge, which can lead therefore to EF overestimation. Thus, Tang et al. (2010) propose a

method more adapted for arid and semi-arid climate regions to estimate the highest surface temperature at each fraction cover interval and subsequently determine both the dry and wet edges. In the same context, a contextual method was applied efficiently in the Sahelian climate in Allies et al. (2020). In this study, the authors have used the EVASPA S-SEBI Sahel (E3S) algorithm adapted from the EVASPA tool (Gallego-Elvira et al., 2013) to obtain more reliable results in these semi-arid regions characterized by the alternation of a dry season and a monsoon period. E3S is an approach that derives ET estimates from a dynamic weighting scheme of ET estimates derived from several EF methods used in previously cited studies. Indeed, it was proven in different studies, mainly for ET estimation, that it is usually better to use an ensemble estimation than any single method in order to consider seasonal and climatic variations (Mueller et al., 2013; Ershadi et al., 2014). However, methods should be weighted according to different sites and seasons in order to enable more realistic estimation. In Allies et al. (2020), method selection was performed using fixed dates for the wet, dry and transition season, without taking the actual hydric state of the surface into account. It also used an empirical approach to assign weights between methods based on the Leaf Area Index (LAI) time series during the transition season. Their study demonstrates that this approach consistently outperforms both non-ensemble and unweighted ensemble methods. However, their methodology relies on in-situ expertise specific to their study area in Southwest Niger, West Africa. As a result, it cannot be easily generalized to other regions without sufficient knowledge of local conditions, making application on other regions or at large scale challenging. To address this limitation, the authors propose weight allocation through objective statistical techniques, such as Bayesian Model Averaging (BMA). However, the frequent lack of ground ET measurements often limits the training of such statistical methods. The aim of this study is to develop a new method, based on the same concept but offering more robust and generalized estimation of wet and dry situations regardless of prior local knowledge about precipitation regimes or vegetative state. This approach will aid in generating more accurate ET estimations with E3S adapted to the actual hydroclimatic conditions of the satellite acquisitions and in limiting the high uncertainty inherent to the determination of wet and dry edges in these situations.

The new approach is based on a sensitivity analysis of the EF with respect to the position of dry and wet edges in order to discriminate adequate EF calculation methods that should be used. The new E3S version is tested in a Sahelian agropastoral area in central Senegal. The objective of this work is therefore twofold: (1) Perform a homogeneity assessment (thermal contrast) regarding surface conditions in the same image, and (2) develop an automatic algorithm to select adequate empirical methods for the definition of dry and wet edges for each detected case.

2. Materials and methods

2.1. Study area

The study was conducted in a meso-site (140×140 km) region in Senegal, West Africa ($13.78^{\circ}N$ to $15^{\circ}N$; $15^{\circ}W$ to $17.09^{\circ}W$; Fig. 1(a)), referred to as "Senegal center" in the study. The site extension corresponds approximately to a Sentinel 2 tile size, which is a good compromise to obtain sufficient heterogeneity and to satisfy the hypothesis of constant climatic behavior as well.

The region is characterized by a tropical semi-arid climate and by the strong temporal and spatial variability of rainfall, with episodic droughts and frequent crop failures (Kizito et al., 2006). The climate is characterized by a rainy season that lasts from June to October and a dry season that lasts from November to May, as presented in the temperature/rainfall ratios graph (Fig. 2). The total annual rainfall in this region is low and highly variable, with less rainfall mainly during the early part of the wet season (Roupsard et al., 2020). The

annual rainfall average is about 585 mm per year over the 1991-2020 period according to in-situ measurements from Fatick station. The mean annual temperature oscillates around 27.7 °C and fluctuates between a maximum average of 35 °C in the month of May and a minimum of 15 °C in the month of January. Most of the area is covered by agro-pastoral plots and Croplands (groundnut, millet, sorghum, cowpea and watermelon), mostly subsistence farming, as part of the Senegal Groundnut Basin (see Fig. 1(b)). Agroforestry is often practiced in this area, which also includes protected natural reserves (Thies and Bandia). The study area is characterized by considerable ecosystemic and hydrologic variability, mainly due to the presence of the Saloum Delta, including mangrove forests. This latter induces different biodiversity dimensions and wide heterogeneous characteristics. The Faidherbiaflux measurement site (Roupsard et al., 2020), in the Niakhar locality, referred to as "Niakhar" later in this study (Fig. 1(a)), provides two different instruments for flux measurement positioned at different heights (4.5 m and 20 m). Therefore, depending on the nearby vegetation type and height, mainly agroforestry plot with millet/groundnut rotation from the groundnut basin, different aerodynamic characteristics are observed at this site.

2.2. EVASPA S-SEBI Sahel (E3S)

EVASPA S-SEBI Sahel (E3S) was developed by Allies et al. (2020) as an adaptation for the Sahelian context. E3S is based on the S-SEBI contextual method (Roerink et al., 2000) and the EVapotranspiration Assessment from SPAce (EVASPA) tool (Gallego-Elvira et al., 2013). In the S-SEBI and E3S models, dry and wet temperatures are retrieved according to albedo values (α) using a scatterplot of the surface temperature and albedo (Fig. 3). However, EVASPA generates an ensemble of ET estimates and the associated uncertainties from the combination of several methods for edge identification.

E3S involves 18 algorithms for wet and dry edge determination (see Table 3 in Annex). The EF estimation is computed based on the S-SEBI model approach, assuming that the EF is the distance between the pixel (i), associated with the α_i value and LST_i value (see Fig. 3), and extreme temperature for wet $(LST_{wet(\alpha_i)})$ and dry $(LST_{dry(\alpha_i)})$ areas that are already defined (see Eq. (1)). Consequently, the LE could be retrieved from the EF and available energy (AE), which corresponds to the difference between the net radiation (Rn) and ground heat flux (G) (see Eqs. (2)-(4)). Eq. (2) represents the portion of available energy allocated to evapotranspiration. Indeed, EF is an indicator of the partition of the available energy between sensible heat flux (H) or evapotranspiration, which is directly related to the water stress state and thus the LST variations. In Allies et al. (2020), MODIS data are used as inputs for E3S. For this aim, Allies et al. (2020) use a cloud edge filtering step in the processing chain to avoid outlier pixels that could distort the surface temperature/albedo (LST- α) scatterplot shape:

$$EF_{LST_{i},\alpha_{i}} = \frac{LST_{dry(\alpha_{i})} - LST_{i}}{LST_{dry(\alpha_{i})} - LST_{wet(\alpha_{i})}},$$
(1)

$$LE = EF * (Rn - G), \tag{2}$$

$$R_n = Rg(1 - \alpha) + \epsilon (Ra - \sigma LST^4), \tag{3}$$

where Rg is the incident short-wave solar radiation, α is the surface albedo, ϵ is the emissivity of the surface, Ra is the incident atmospheric radiation and σ is the Stefan–Boltzmann constant (5.67 10^{-8} W m⁻² k⁻⁴).

$$G = R_n * (0.4 - (0.33 * NDVI)), \tag{4}$$

(Kustas and Norman, 1999) where NDVI is the normalized difference vegetation index.

In order to adapt to the Sahelian context, Allies et al. (2020) apply a weighting scheme to identify appropriate EF methods, depending on

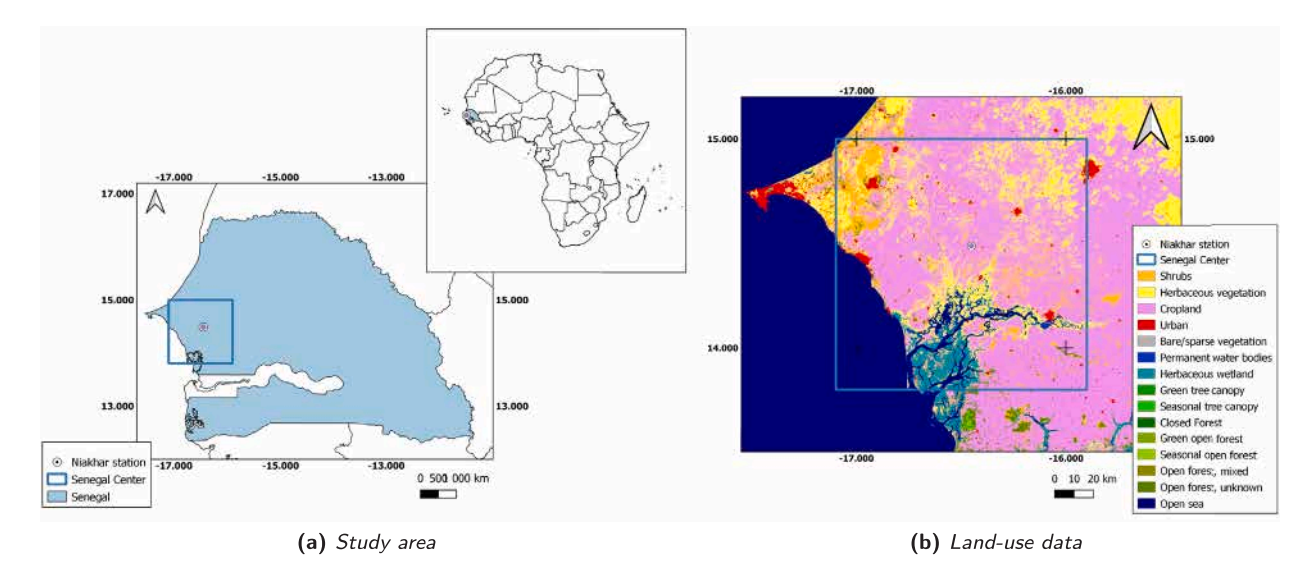


Fig. 1. Study area and land-use data from Copernicus 2019.

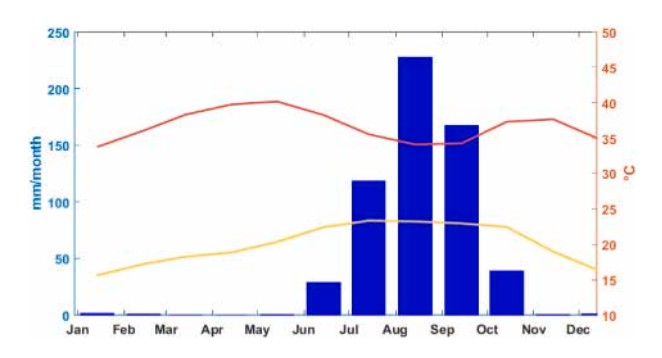


Fig. 2. Maximal (red) and minimal (yellow) temperature and precipitation (blue) at Fatick (1991–2020). (For interpretation of the references to color in this figure legend, the reader is referred to the web version of this article.)

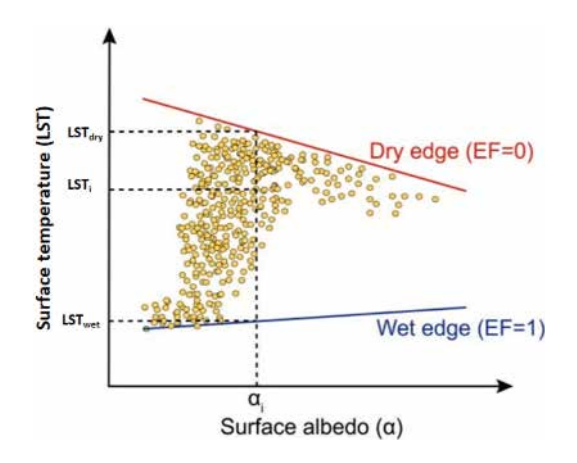


Fig. 3. The relationship between the surface albedo, surface temperature and evaporative fraction based on the S-SEBI method (Allies et al., 2020).

the stage of the seasonal cycle. In fact, the strong seasonality observed in the Sahelian region leads in many cases to a lack of dry and wet pixels in wet and dry seasons, respectively. This, in turn, leads to incorrect estimates of the dry and wet edges. To overcome this issue, Allies et al. (2020) introduced additional edge determination algorithms denoted as "dry methods" and "wet methods" in the E3S model (see Fig. 4). "Dry methods" involve the determination of a theoretical wet edge fixed at the minimal observed LST (LST_{min}). These methods are used

in the dry season, when there is a lack of wet pixels within the image that can be used to determine the wet edge accurately. In a similar way, "wet methods" use a theoretical dry edge fixed at the maximal observed LST (LST_{max}) in the wet season. During the transition period, which is between the end of the wet season and the beginning of the next dry season, the classical edge determination methods of EVASPA are also used given the simultaneous presence of sufficient dry and wet pixels during this period. In Allies et al. (2020), the MODIS LAI product was used as a weighting variable to distinguish between the different seasons. Indeed, the LAI is a reliable proxy for the surface water status.

2.3. Input data

- MODIS data: The model requires the LST and optical properties of the surface cover as inputs. Thus, we use remotely sensed data from the latest collection (6) of 1-km-resolution MODIS TERRA/AQUA products, available at http://earthexplorer.usgs. gov. The temporal 16-day composite series of the MODIS normalized difference vegetation index (NDVI) (MOD13A2/MYD13A2 from the satellites TERRA and AQUA, respectively), daily LST, surface emissivity (ϵ) and viewing angle (MOD11A1/MYD11A1 from TERRA and AQUA, respectively) and daily albedo (α) series (MCD43A3) with a spatial resolution of 500 m are used. These data are acquired for our study period (2018-2021), at the resolution of the MODIS sensor of 1 km. Therefore, the temporal interpolation of NDVI data and the spatial aggregation of albedo data are performed in order to obtain daily information corresponding to the satellite overpass and the same spatial resolution. Mostly, the TERRA product is used. The AQUA product is used for days when the TERRA product is not available.
- ERA5-Land meteorological data: ERA5-Land Muñoz-Sabater et al. (2021) climate reanalysis data are used to provide hourly global radiation (Rg) and atmospheric radiation (Ra) time series at a spatial resolution of 9 km to be used as inputs for E3S. ERA5-Land is an enhanced global dataset for the land component of the fifth generation of European ReAnalysis (ERA5) data. Indeed, in comparison with previous ERA5 products, ERA5-Land involves several updates to support land monitoring applications, mainly by re-running its land surface scheme at a finer spatial resolution based on ERA5 forcing (from 31 km to 9 km) (Muñoz-Sabater et al., 2021). The key advantage of using ERA5-Land is the temporal consistency and the long and continuous period of availability of the data, from 1950 until now. Our meso-site (Fig. 1(a)) lies across several ERA5 grid cells.

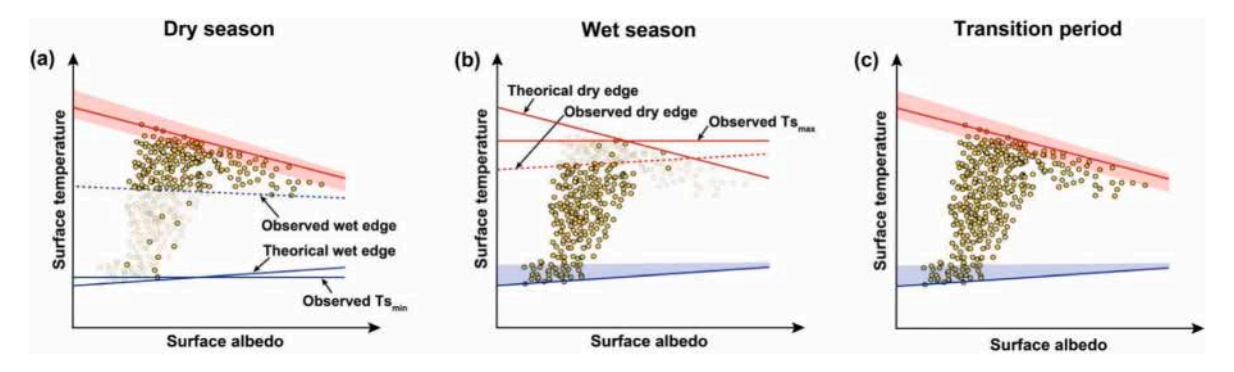


Fig. 4. LST- α scatterplot configuration during the dry season (a), the wet season (b) and the transition period (c) (Allies et al., 2020).

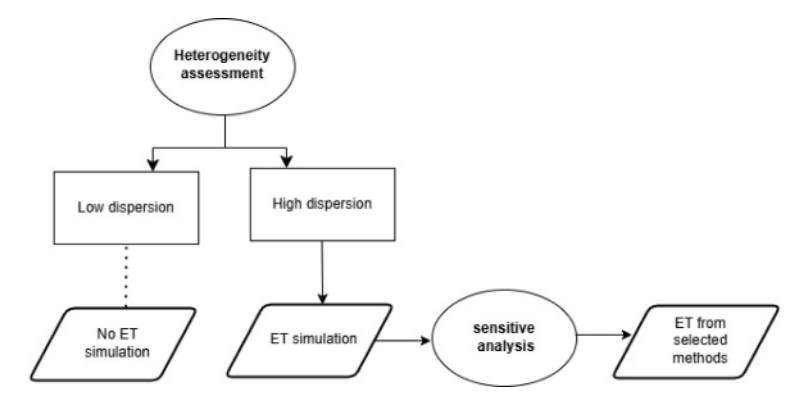


Fig. 5. Analysis flowchart.

2.4. Automatic edge selection method: E3S new version

E3S New version is based on Allies et al. (2020)'s adaptation for the weighting scheme and cloud edge filtering. Our purpose is to generalize the native E3S method in order to allow it to be used without prior knowledge of the study area characteristics and season allocation. For this aim, sensitivity analyses will be particularly useful to (1) evaluate the assumption of having sufficiently wet and dry pixels within the same image and (2) implement a systematic selection for adapted methods of EF estimation for different cases (see Fig. 5).

2.4.1. Heterogeneity assessment

One of the most important hypothesis behind contextual methods is that the perceived LST heterogeneity covers the entire spectrum of water stress conditions, from fully dry to fully wet. In order to measure LST dispersion, we have used the difference between the maximum and the minimum of the relative median absolute deviation (MAD). The MAD computes the deviation of scores from the overall median (Eq. (5)) to obtain the lowest and highest absolute distance to be used as an estimation of the dispersion. This is widely used as a robust measure of quantitative variable dispersion since it relies on the median to estimate the distribution center (Arachchige et al., 2022). Hence, it does not rely on the assumption that the LST samples follow a normal distribution. Besides, MAD is known to be more resilient to outliers (Chen and Liu, 2020), which makes it particularly useful for identifying the maximum contrast needed to satisfy the method's assumption. Furthermore, the Relative MAD (MAD divided by the median) provides a scale-independent measure of dispersion rather than an absolute difference, making it suitable for comparing LST variability across different regions and time periods. A minimal relative MAD threshold should ensure that the sufficient heterogeneity requirement of E3S is met. Its determination is described in Section 2.4.3:

$$Relative MAD = \frac{|x_i - median|}{median}.$$
 (5)

2.4.2. Selection of adapted edge determination method

For each image, if the heterogeneity assumption is validated, we have to detect the positioning of the LST- α point cloud regarding the limiting boundaries identified according to the different EF determination methods. This assessment is particularly useful for identifying specific situations, making it possible to characterize the point cloud's behavior. For this aim, we calculated the derivative of the EF with respect to LST_{dry} , denoted " dEF_{dry} ", and the derivative of the EF with respect to LST_{wet} , denoted " dEF_{wet} " (Eqs. (6) and (7), respectively). Indeed, following Eqs. (6) and (7), these derivatives tend toward zero when the distance to the considered edge increases. This method thus allows the detection of the general positioning of the point cloud with respect to the edges and the selection of adequate edge determination methods:

$$dEF_{dry} = \frac{\partial EF}{\partial LST_{dry}} = \frac{LST - LST_{wet}}{(LST_{dry} - LST_{wet})^2},$$
 (6)

$$dEF_{wet} = \frac{\partial EF}{\partial LST_{wet}} = \frac{LST_{dry} - LST}{(LST_{dry} - LST_{wet})^2}.$$
 (7)

A homogeneously dry situation is observed when there are more hot pixels than cold pixels; they are mainly stacked toward the dry edge, as observed in Fig. 4a. With EF methods adapted to dry situations, the points should also be far from the wet edge, that would be closer to the theoretical wet edge than with unsuitable methods. This situation is easily identified when " dEF_{wet} " for dry-adapted methods has a very low value tending toward zero, with a simultaneously high value of " dEF_{dry} " tending toward ($1/LST_{dry}-LST_{wet}$). On the contrary, a homogeneously wet situation is observed when $LST-\alpha$ points are mainly stacked up on the wet edge, as observed in Fig. 4b. Points should also be far from the dry edge with wet-adapted methods in this case. It can thus be identified with high " dEF_{wet} " values, tending toward ($1/LST_{dry}-LST_{wet}$), and " dEF_{dry} " values tending toward zero for wet-adapted methods. This difference of behavior between dry-adapted and wet-adapted method regarding " dEF_{dry} " and " dEF_{wet} " should allow

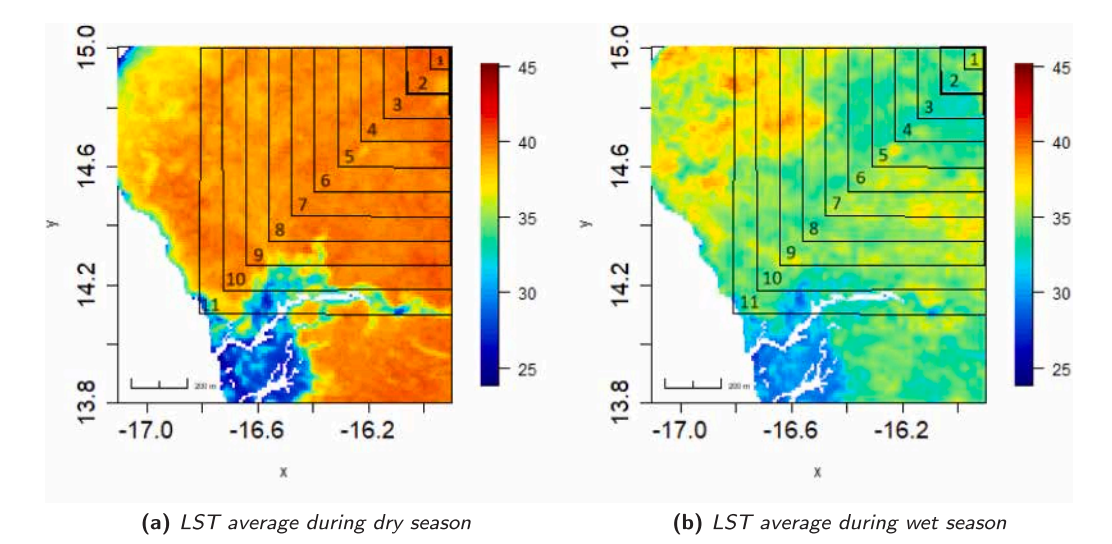


Fig. 6. Spatial variability of LST average according to the season over the different expanding windows (presented from 1 to 11).

for an identification of dry and wet situations and select only the adapted methods. A sufficiently heterogeneous situation is identified when we obtain simultaneously high " dEF_{wet} " and " dEF_{dry} " values, indicating high variability around both dry and wet edges (see Fig. 4c).

2.4.3. Threshold definition

Thresholds must be determined (1) to evaluate the dispersion of the LST- α scatterplot and (2) to discriminate among the different situations, as shown in Fig. 4. For this aim, temporal and spatial analyses of our study area were used:

- · Spatial analysis: Spatial analyses are performed using an expanding window in order to sample the widest variety of thermal heterogeneity levels possible in the study area. The objective is to sample a rupture in heterogeneity levels, by taking advantage of local knowledge on the study area. Indeed, estimating dispersion measures across expanding windows, ranging from a very homogeneous sub-area to a highly heterogeneous one (see Fig. 6), is particularly useful to identify the possible range of relative MAD values and set the threshold value just below the rupture of homogeneity. In this study, 14 sub-areas are defined using a 10 km increment in window size. The position and size of the windows is set to gradually increase the thermal heterogeneity level of the scene. The homogeneity rupture is then induced by the presence of wetlands, the Saloum delta, which provide sufficient thermal contrast for robust E3S estimates. From this, an adequate dispersion threshold to be used for heterogeneity assessment can be identified.
- Temporal analysis: The chronological variation of the derivatives
 of the EF (using non-exceedance frequency) is very informative
 for defining a specific behavior according to different water states
 and therefore for choosing thresholds to be used to identify the
 different situations mentioned in Section 2.4.2.

3. Results

3.1. Dispersion assessment

The dispersion coefficient (see Section 2.4.1) is computed according to different sub-areas and for different seasons during our study period (Fig. 7). The aim of this analysis is to identify which LST dispersion value best identifies sufficient surface heterogeneity. Overall, the dispersion coefficient calculated from the first expanding windows (from the 1st to the 8th sub-area, Fig. 6) presents a relatively steady variation

and lower values, not exceeding 2. However, beyond the 8th expanding window, the dispersion coefficient increases sharply for the different seasons and reaches values greater than 2. This means that a high LST dispersion is observed when the 8th expanding window is reached. The LST spatial variability observed in Fig. 6 strengthens our findings: The LST is observed with no significant variation using the first subareas in the dry or wet season. However, some colder and hotter pixels are observed in the 8th sub-area, respectively, in Figs. 6(a) and 6(b). Mainly, the coldest pixels observed in the dry season are induced by the presence of the Saloum Delta, and the hottest pixels are induced by the farming area (Fig. 1(b)). These pixels are able to provide sufficient heterogeneity conditions in the scene. Consequently, for this study case, if the dispersion coefficient is greater than 2, it can be assumed that the LST dispersion is sufficiently heterogeneous, allowing the use of the E3S model (see Appendix B.1 in the Annex).

3.2. Thresholds estimation for dry and wet situations detection

In order to accurately identify dry and wet situations observed in Fig. 4, dEF_{drv} and dEF_{wet} will be used as indicators to determine the general position of the $LST - \alpha$ scatterplot with respect to the wet and dry edge positions. As explained in Section 2.4.2, dry-adapted and wet-adapted methods should have different behavior regarding these derivatives indicators in wet and dry situations. For this purpose, thresholds must be defined to distinguish the behavior of dry-adapted and wet-adapted EF methods in both dry and wet situations and select only the most suitable methods for the current situation. For that purpose, the cumulative distributions of dEF_{drv} and dEF_{wet} for all EF methods across the entire image are analyzed in typical dry and wet situations. These distributions are presented in Fig. 8 for a typical day from the dry season (March 9, 2018) (Figs. 8(a) and 8(b)) and for a typical day from the wet season (September 19, 2018) (Figs. 8(c) and 8(d)). Lower derivative values mean that the distance between the point cloud and the considered edge is relevant. Adversely, higher derivative values mean that the points are mainly stacked toward the considered edge, and there is a higher rate of change around this edge. Overall, Fig. 8 shows that dEF_{dry} and dEF_{wet} exhibit different behaviors depending on the type of method used for edge estimation (i.e. dry, wet or transition method, cf. Section 2.4.2) and the season. For the dry season, results show that dEF_{dry} (Fig. 8(a)) and dEF_{wet} (Fig. 8(b)) estimated from dry methods (black lines), i.e., using a theoretical wet edge in order to reach the coldest pixel in the image, display different behavior from dEF values estimated from other methods. On one hand, 80% of the dEF_{wet} values from adapted dry methods are very low (less than

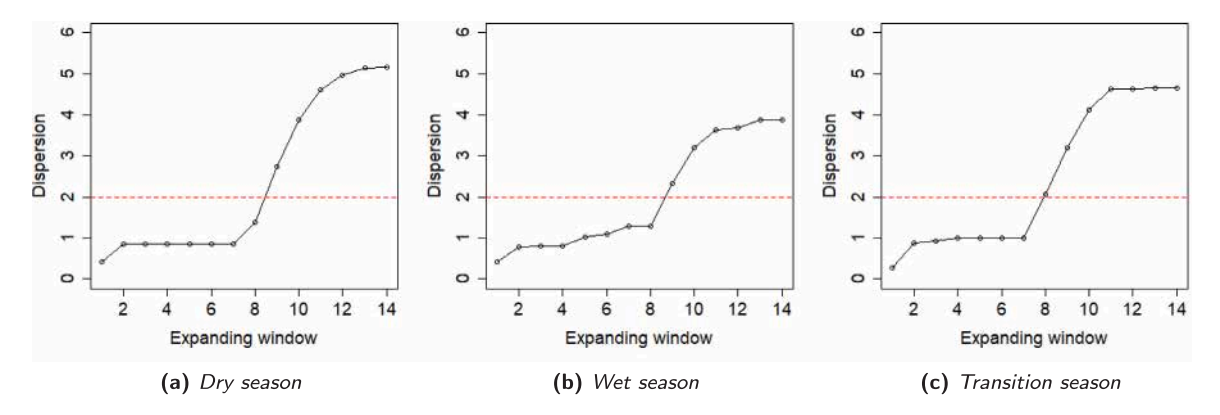


Fig. 7. LST dispersion according to expanding windows and seasons.

Table 1 Thresholds used to define the different $LST - \alpha$ scatterplot configuration.

	$dEF_{dry} > 0.03$ adapted method for dry situation	$dEF_{dry} < 0.03$ adapted method for wet situation
$dEF_{wet} < 0.01$ adapted method for dry situation	Homogeneously dry situation	х
$dEF_{wet} > 0.055$ adapted method for wet situation	х	Homogeneously wet situation

0.01), which indicates a large distance to the wet edge (Fig. 8(b)). On the other hand, 50% of the dEF_{dry} values, also from dry methods, present higher values, greater than 0.03, which highlights the shorter distance to the dry edge (Fig. 8(a)). This situation could be identified as a "homogeneously dry situation", as explained in Section 2.4.2; dEF_{wet} presents very low values tending toward zero, with simultaneously higher values of dEF_{dry} . However, 50% of the dEF_{wet} and dEF_{dry} values obtained using other methods present higher values exceeding 0.05 in almost all cases, which hints at a well-scattered LST – α scatterplot between the two estimated limiting edges, meaning that the edges are closer to each other than they should be theoretically. It indicates a typical dry situation, as shown in Fig. 4a, where dry methods and other methods have a significantly different wet edge position. Similarly, for the wet season, dEF_{dry} (Fig. 8(c)) and dEF_{wet} (Fig. 8(d)) estimated from wet methods (orange lines), i.e., using a theoretical dry edge in order to reach the hottest pixel in the image, indicates a significantly different position of the wet edge than other methods, showing a typical wet situation, as shown in Fig. 4b. Indeed, 50% of dEF_{dry} values obtained using wet methods present lower values not exceeding 0.03, which indicates a great distance to the dry edge (Fig. 8(c)). Meanwhile, 50% of dEF_{wet} values show higher values, greater than 0.055 (Fig. 8(d)). This situation could be identified as a "homogeneously wet situation" (see Section 2.4.2), with high dEF_{wet} values and dEF_{dry} tending toward zero. Based on these findings, in this work, we can use the already identified thresholds for these typical days from the dry and wet seasons, mentioned also in Table 1, in order to define the different situations shown in Fig. 4. More results to validate the thresholds values identified are observed in the Annex (Appendix B.2).

3.3. EF method selection

3.3.1. Simulation before and after method selection

In what follows, "ALL" and "E3S-V2" refer, respectively, to the ET simulations using E3S with all the available methods and the new version of E3S with the suggested automatic method selection. "Obs" refers to in-situ measurements at the Niakhar flux station. "Obs" are presented using an envelope corresponding to the minimal and maximal values of the two eddy-covariance instruments (Fig. 9), while the central value is their mean. The use of observation values derived

from two different gauging station is helpful to provide a realistic representation of MODIS pixel. Indeed, using only the lowest station for example, does not include the trees that characterize the observed ecosystem. Error bars using the 25th, 50th and 75th percentile values of "ALL" and "E3S-V2" are used to express the related uncertainties.

Overall, in Fig. 9, the "ALL" simulations overestimate ET compared to "Obs" during the dry season and underestimate it during the wet season (Fig. 9). However, using only selected methods, provided by the "E3S-V2" simulations, leads to the correction of both the overestimation and underestimation and minimizes the dispersion initially observed in the "ALL" simulations. Consequently, uncertainty linked to the method ensemble is considerably reduced, providing ET estimation that follows the ground truth estimates more closely. In the wet season, few data are available for ET estimation due to the presence of clouds. Nevertheless, on some days, where data are available, the method selection step succeeded in improving the ET estimation. On the other hand, at the beginning of the transition period, when the $LST - \alpha$ scatterplot did not identify a "homogeneously dry situation" or a "homogeneously wet situation", all the EF methods correctly reproduce "Obs". However, at the end of the transition season, when vegetation is sparser and the number of wet pixels decreases, the "E3S-V2" simulations underestimate ET compared to the "Obs" mean but remain within the measurement interval. Indeed, the selection algorithm tends to select methods adapted for the dry season during this period.

In order to analyze the spatial patterns of ET, maps of the seasonal ET average corresponding to the "ALL" and "E3S-V2" simulations are presented in Fig. 10. Figs. 10(a) and 10(b) show estimates for dry seasons observed during the whole study period, while Figs. 10(d) and 10(e) show estimates for wet seasons. Figs. 10(c) and 10(f) show the difference between "ALL" and "E3S-V2" in both cases. The results for the dry season show that ET values from the "ALL" simulations are overestimated compared to those of "E3S-V2". Fig. 10(c) shows positive differences all over the study area. Moreover, differences are more pronounced in the coastal region, around the Saloum Delta and in some cultivated zones. Indeed, these regions have the coldest pixels, with relatively low temperature values (see Fig. 6(a)). As the true wet edge cannot be identified correctly with methods unsuitable for the dry season, the "ALL" simulations include overestimated wet edges. Consequently, the EF will be significantly overestimated, leading to higher ET rates, with differences exceeding 1 mm d⁻¹. Smaller differences are

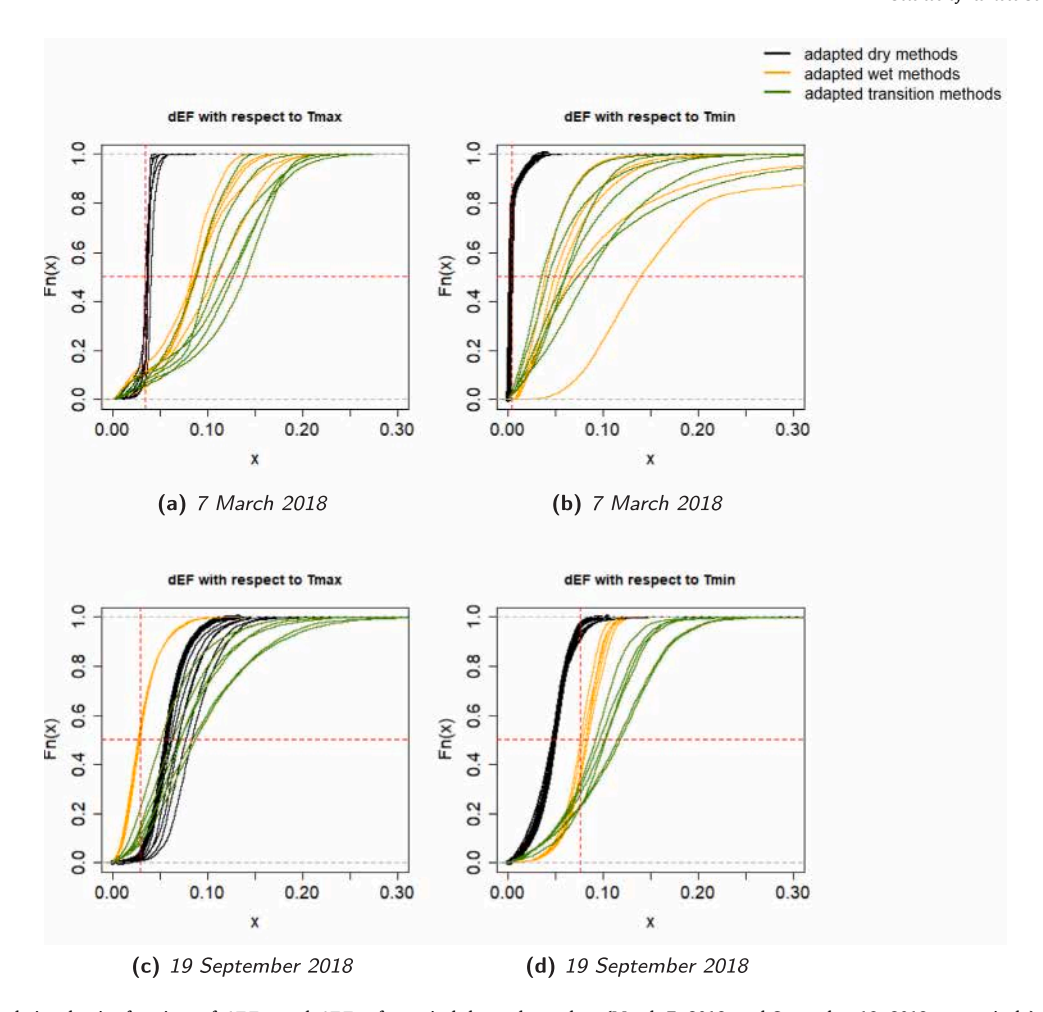


Fig. 8. Empirical cumulative density functions of dEF_{dry} and dEF_{dry} for typical dry and wet days (March 7, 2018, and September 19, 2018, respectively). (For interpretation of the references to color in this figure legend, the reader is referred to the web version of this article.)

found in crop ecosystems, which have higher temperatures due to the presence of bare soil. Indeed, EF estimations for drier points are less sensitive to the position of the wet edge (Eq. (7)), leading to smaller differences in ET.

Conversely, the results for the wet season show that the "ALL" simulations have slightly lower values than the "E3S-V2" simulations on average. Unlike the dry season, the spatial patterns of the differences (Fig. 10(f)) are more homogeneous, with a relatively constant difference of around 0.5 mm d $^{-1}$. Differences are more visible in the southeast part of the study area, with more intensive crop management and forests. Lower differences are found for the coldest pixels, as their EF is less sensitive to the estimation of the dry edge (see Eq. (6)). Few zones yield higher differences (around 0.5 mm d $^{-1}$) for the hottest pixels, which are more sensitive to dry edge estimation.

3.3.2. Comparison with reference products

Comparisons with the native version of E3S used in Allies et al. (2020) show that the E3S-V2 have conserved the initial performance observed in the original version. Fig. 11(b) shows that E3S-V2 and the native version have a similar variation when compared to simulations with the mean ET from observations, mainly in the dry season. Because of the use of thermal infrared information, the available data derived from model simulations in the wet season are insufficient for comparison. However, during the transition season, simulations from E3S-V2 follow the observations more closely, while ET from the native version shows underestimation. Fig. 11(a) strengthens our findings; the E3S-V2 and native E3S simulations show high performances in comparison with ET derived from measurements, with R-squared values exceeding 0.6

and relatively low RMSE values. Moreover, simulations from E3S-V2 fit the observations more closely, with a higher R^2 value (around 0.74) and a lower RMSE value (around 0.47 mm d^{-1}) compared to the native version of E3S, which presents a lower R^2 (around 0.64) and an RMSE value of about 0.64 mm d^{-1} . The E3S-V2 is not only able to conserve the performance observed initially using the native version of E3S but also reproduces the observations better.

Fig. 12 shows the comparison between E3S-V2 simulations with ET values derived from other ET products, retrieved for the Niakhar pixel, presenting good performances in the African continent and mainly in the Sahel region (Trambauer et al., 2014; Etchanchu et al., 2025): the ERA5-Land and GLEAM products (see Annex A.1). Overall, ET values from the different products show comparable performances. The ET time series from ERA5-Land show lower values mainly in the dry season, in comparison with ET from Gleam product and "E3S-V2" simulation. The two latter present mainly similar temporal variations at local scale. This could explains the higher correlation value obtained at mesoscale (Table 2), around 0.73, between "E3S-V2" and Gleam product. However, lower R^2 value, around 0.63, is observed between "E3S-V2" and ERA5 Land product (Table 2). Nevertheless, comparisons at mesoscale in Fig. 13, show more differences between "E3S-V2" and Gleam product (Fig. 13(a)), inducing relatively higher bias and RMSE values, around 0.3 and 0.43 mm d⁻¹ respectively (Table 2). Higher differences are also observed between "E3S-V2" and ERA5 Land product, mainly for some lower values (Fig. 13(b)), which leads to higher bias and RMSE values around 0.43 and 0.64 mm d⁻¹ respectively (see Table 2).

A spatial analysis is carried out to compare ET estimates from "E3S-V2" with ET values from other models (the native version, the

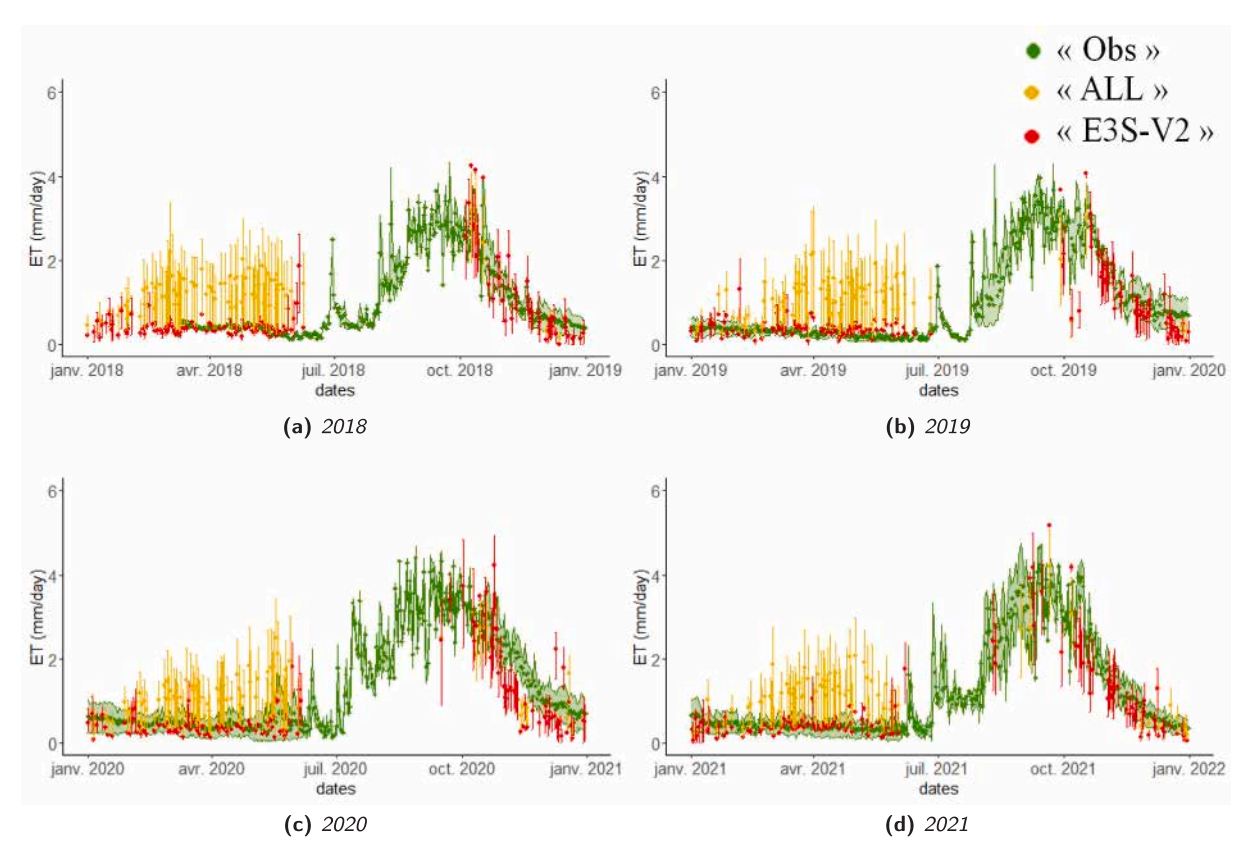


Fig. 9. Comparison of LE simulations using "ALL" and "E3S-V2", with the LE from "Obs", using different in-situ measurements at the Niakhar station pixel.

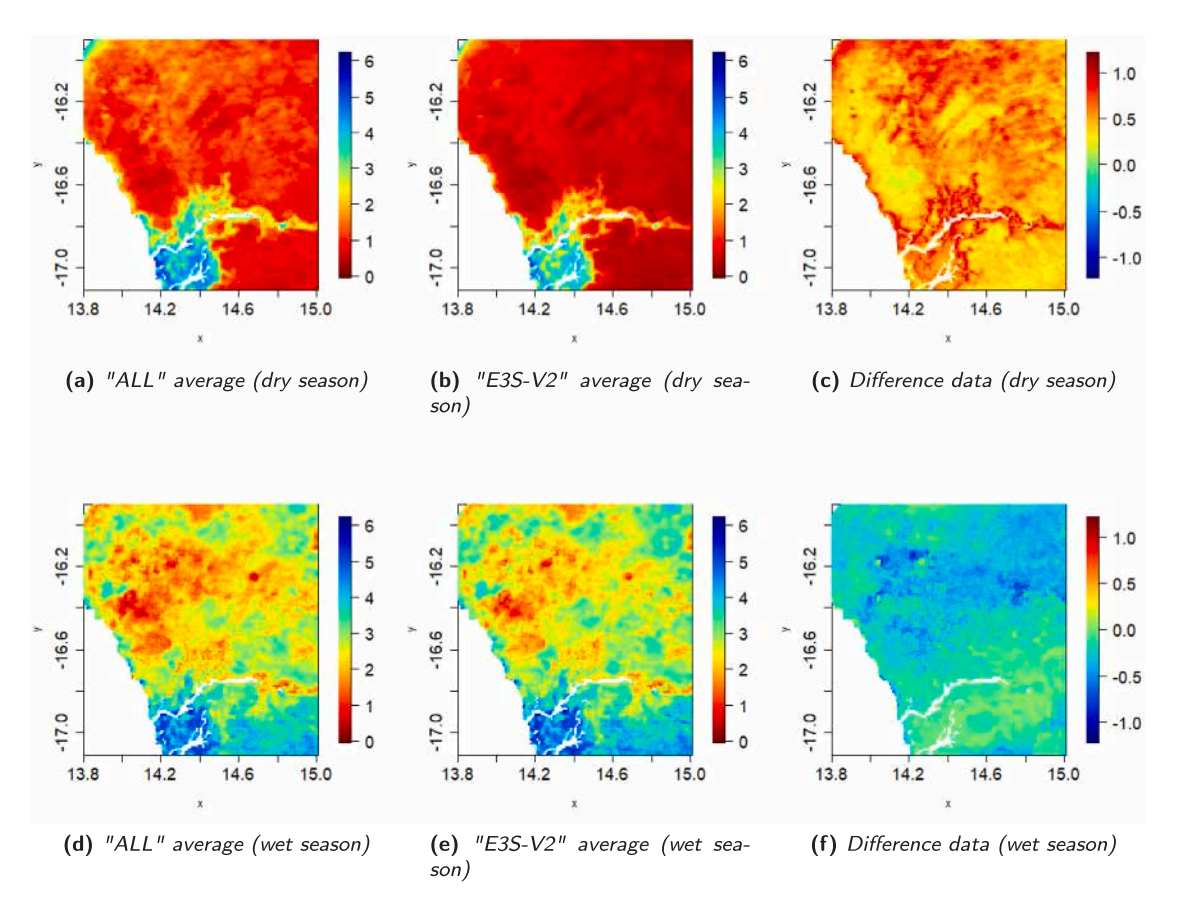


Fig. 10. ET seasonal average data using "ALL" and "E3S-V2" simulations during the wet and dry seasons over the whole of the study period.

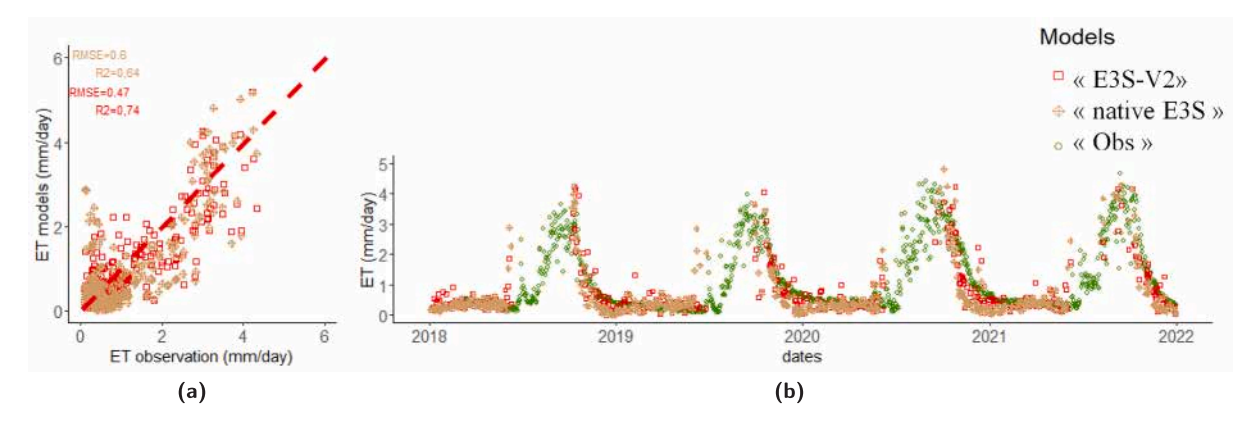


Fig. 11. Comparison of ET (mm/day) from "E3S-V2" simulations with ET from the native E3S method (Allies et al., 2020) and the mean ET from observations (a, b) at locale scale (Niakhar pixel).

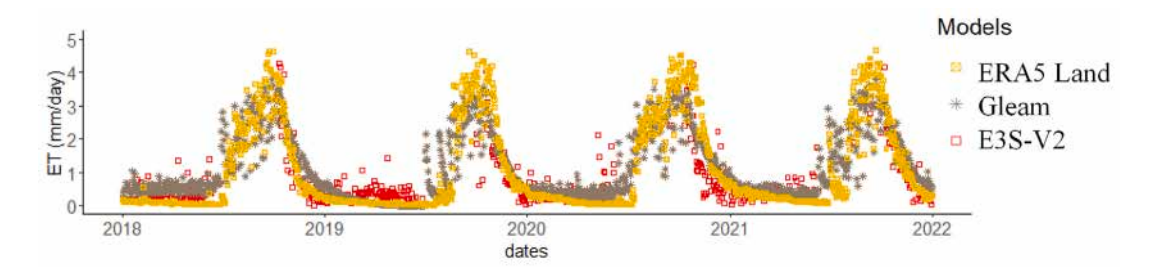


Fig. 12. Temporal variation of ET from "E3S-V2" and reference ET products in the study area: Gleam and ERA5 Land, retrieved for the Niakhar pixel.

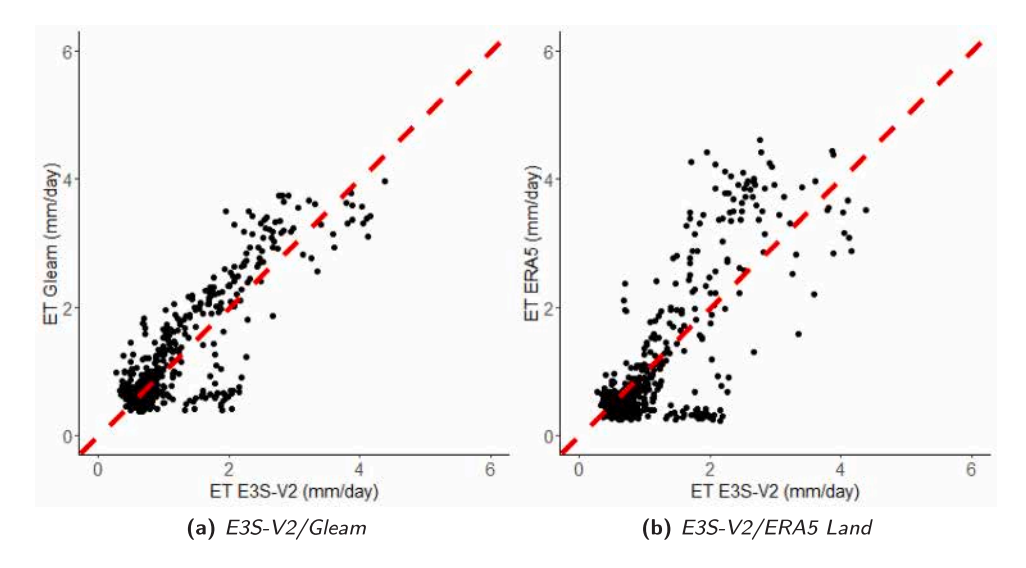


Fig. 13. Comparison of mean ET (mm/day) over the area between "E3S-V2" simulations and reference ET products in the study area: Gleam and ERA5 Land.

Table 2 Statistical indicators (Bias, R^2 and RMSE) on mean ET temporal series over the entire area between "E3S-V2" simulations and the different ET products used for comparison: Gleam and ERA5 Land.

	E3S-V2/Gleam	E3S-V2/Gleam E3S-V2/ERA5 Land	
Bias (mm d ⁻¹)	0.3	0.43	
R^2	0.73	0.63	
RMSE (mm d ⁻¹)	0.43	0.64	

ERA5-Land and GLEAM products). Firstly, an up-scaling procedure is performed in order to be able to compare these different products (see in Annex, Appendix A.3). Secondly, the R^2 , RMSE and bias scores between each ET product and ET from E3S-V2 are computed for each

pixel and presented in Fig. 14 for the whole study period. The native version and E3S-V2 simulation, which have the same spatial resolution (kilometric scale), provide closer estimates over the whole study area. Indeed, they have higher correlation, with an R^2 value around 0.7 over almost the whole study area (see Fig. 14(a)). Moreover, Figs. 14(d) and 14(g) show very low RMSE and bias scores, about 0.5 and -0.5 respectively in almost all the study area. However, differences become more accentuated around the Saloum Delta and coastal pixels, exceeding 3 mm d $^{-1}$ of RMSE and -3 mm of bias value. This means that ET values from E3S native version, under-estimate ET values provided from E3S-V2 in these regions. The comparison with ERA5-Land product, available at a lower resolution than E3S-V2, shows more heterogeneous correlation values (Fig. 14(b)). In fact, very low R^2 scores, lower than 0.4, are observed in wetland regions and also in the North-West of the study

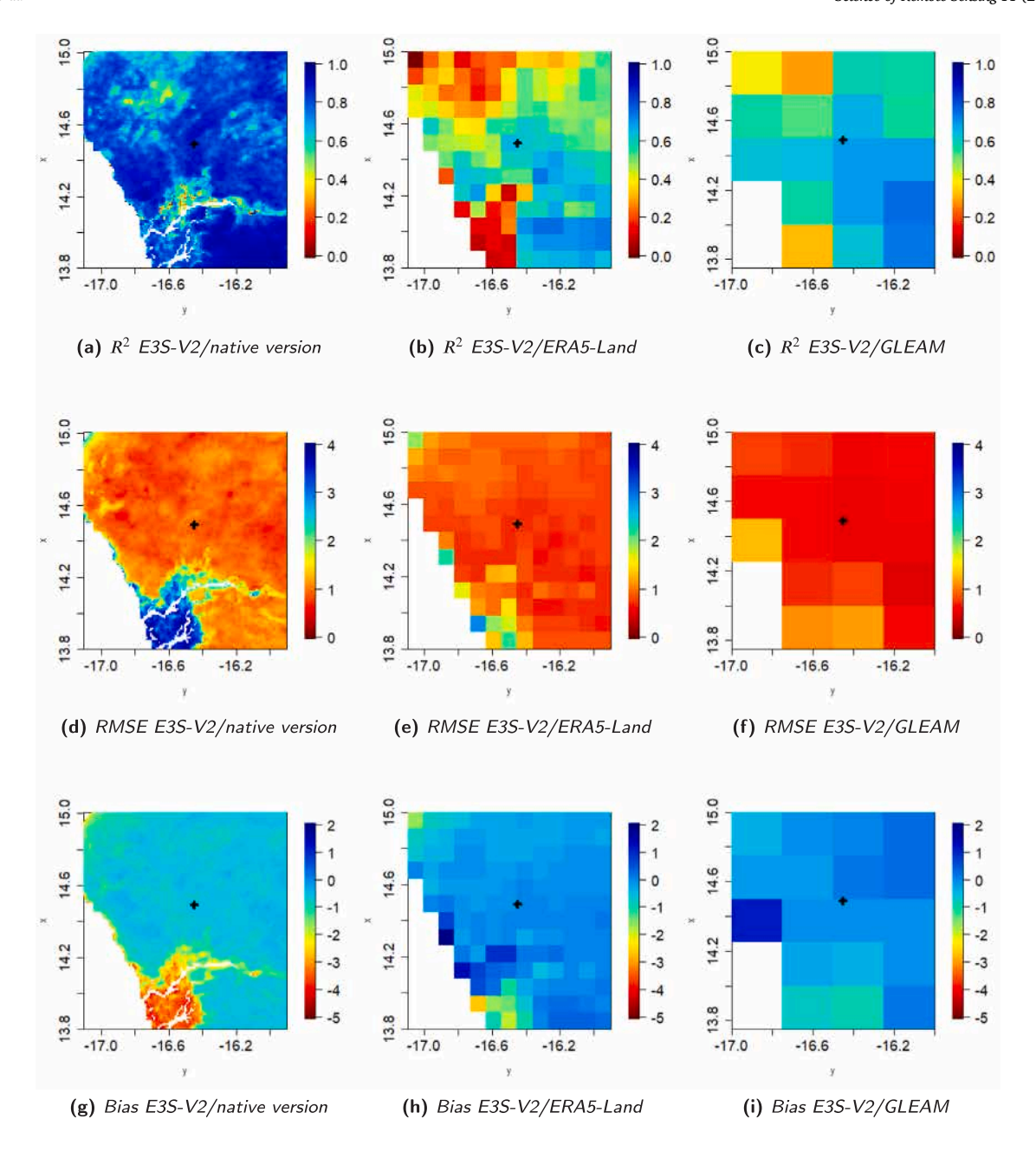


Fig. 14. Statistical indicators (Bias, R2 and RMSE) data calculated using simulated ET from E3S-V2 and ET derived from different products: ERA5-Land, GLEAM and E3S native version, at spatial scale. Niakhar station is located in the data.

area. Higher R^2 scores are observed in cultural regions. Nevertheless, the RMSE and bias data indicate more homogeneous difference values, nearly 0.5 mm d⁻¹ over the whole study zone. Larger differences are observed in coastal pixels and mainly in wetland areas, exceeding, for some pixels, 2 mm d⁻¹. These differences could explain therefore low RMSE and bias values performed at meso-scale and presented in Table 2. Comparisons with the GLEAM products, which have the lower spatial resolution, show mainly similar performances than ERA5 Land at spatial scale. However, better correlation values than ERA5-land are observed when using Gleam product, which consolidates the mesoscale R^2 value observed in Table 2. Nevertheless, Figs. 14(f) and 14(i) show the lower RMSE and bias values calculated in wetland areas, with differences of around 1 mm d⁻¹ only. This means that E3S-V2 have similar performances as Gleam product in wetland regions, which are the more challenging zones to estimate.

4. Discussion

The results of our work show the potential of the proposed method to enhance the accuracy of ET estimation during the study period. Indeed, the seasonality is well represented, with low evapotranspiration during dry periods, high rates of evapotranspiration in the wet season and variable rates that decrease gradually during the transition season. Moreover, we have succeeded in significantly reducing the structural uncertainties observed initially, i.e., before the method selection. Simulations are compared with observations provided from two different gauging stations installed at our flux site. ET measurements show a noticeable difference between both instruments (Fig. 9), explained by their different measurement height. This latter involves different footprint size, inducing different land use. This variability seems to be representative of MODIS pixel mainly in transition period, where

vegetation presents higher evolution dynamic. Indeed, ET from "E3S-V2" is almost always within the observation envelope presenting the higher and the lower ET measurement (Fig. 9).

The aim of this work is to generalize the native version of E3S based mainly on local knowledge of the study area. The comparison with the native version shows that the new proposed method conserved the performance of the initial version of E3S, especially in the dry and wet seasons. However, in the transition season, the new method outperforms the initial version without using additional information. Indeed, the native E3S version uses a weighting scheme over the transition period, depending on the water availability, represented by the vegetation canopy structure (LAI). The aim of this approach is to reproduce the theoretical gradually evolving surface state in order to choose appropriate EF methods according to the vegetation cycle. However, the vegetation information almost always provides a delayed response to the surface hydric state. Since the EF method selection proposed in this work is based only on instantaneous information derived from thermal and land surface properties, it accounts better for the actual water availability. Moreover, the use of information provided only from $LST - \alpha$ makes the approach applicable even in areas where there is no well-defined rainy season, without the need for prior local information. The method used for EF selection in the native version of E3S could be the reason for the systematic underestimation observed in the transition period (see Fig. 11(b)). This could as well, explains the high RMSE and bias values observed in wetland areas in comparison with E3S-V2 simulations at spatial scale (see Figs. 14(d) and 14(g)).

E3S-V2 has a good agreement at local scale compared with other products known as a reference in our study area (GLEAM and ERA5-Land) (Allies et al., 2020; Etchanchu et al., 2025). However, comparisons at mesoscale, show more discrepancies between E3S-V2 and ET from other products, inducing relatively high RMSE and bias values. According to spatial representation of statistical scores in Fig. 14, these differences occur mainly in wetland, North-West and coastal regions. Indeed, in the north-west of the study area, lower surface temperature values than the rest of the area during the dry season and higher temperature values in the wet season are observed in Fig. 6. This fact is potentially related to topographic effects inducing shallower soil depth. This leads in turn to lower water storage in the soil and therefore to drier areas in wet season. In dry season, the higher altitude could make this area colder. However, Gleam and ERA5 Land ET products were unable to detect this specific behavior, unlike E3S-V2, that provides higher and lower ET rates respectively in dry and wet season in this region (figures not shown). This explains consequently lower correlation observed in Figs. 14(b) and 14(c) in the north-west region. Differences in ET estimation using these different models might be related to their different spatial resolution. Therefore, higher resolution data (kilometric scale for our case) provide more accurate estimations at spatial scale. Nevertheless, Gleam product presents comparable ET estimation to E3S-V2 in wetland region unlike ERA5 Land product. This could be related to the use of a different land surface model for ET estimation in the ERA5-Land, which is unable to account for the water supply from processes other than precipitation. On the contrary, ET from E3S-V2 and Gleam product are more correlated since they rely on remote observations to describe the surface states e.g., moisture content or surface temperature for more realistic ET estimation. Moreover, such models may estimate fluxes using methods that need much less knowledge of soil and vegetation characteristics than ERA5-Land. Finally, small discrepancies observed in coastal regions are explained by the low spatial resolution of GLEAM and ERA5 Land in comparison with the MODIS products used as inputs for the E3S model.

Uncertainties are induced mainly by the EF method selection (Olioso et al., 2023; Mwangi et al., 2024) when the limiting edges are overestimated or underestimated. This is particularly highlighted for ET data estimation in Fig. 10. In fact, an insufficient number of cold pixels, for instance, in homogeneously dry situations, is problematic for correct wet edge estimation. Similarly, an insufficient number of

hot pixels in a homogeneously wet situation induces the incorrect estimation of the dry edge. Moreover, some consistent EF method estimates are based on quantiles, which leads to the removal of extreme "cold/hot" values and the loss of useful contrasting information that in reality satisfies the contextual models' assumptions. Consequently, it is crucial to identify the specific scenes that require adapted EF calculation methods. For this aim, " dEF_{dry} " and " dEF_{wet} " are found to be powerful indicators that can be used to discriminate among these different situations. Furthermore, one of the key advantages of using the derivative as an indicator is its independence from LST absolute values, which can vary significantly depending on climatic conditions. Indeed, " dEF_{dry} " and " dEF_{wet} " characterize relative changes based only on the distance observed to the limiting boundaries, rather than the absolute temperature positioning. This property makes it a valuable tool for identifying the sensitivity to the dry or cold edges estimations, and therefore for identifying heterogeneity condition in each case. Consequently, this method can also be consistent across various climatic contexts, including warm arid environments, as well as temperate and tropical zones. However, it may not be effective in boreal climates throughout the year. Indeed, at very low LST values, the thermal state is no longer driven by soil moisture conditions but rather by phase changes (freezing and thawing). In addition, in these regions, very low solar radiation and surface energy exchanges do not generate sufficient surface contrast to satisfy the model's assumption. The method's assumption is based as well on the assessment of heterogeneity through LST dispersion measurement. A relative metric was used for this purpose, which also contributes to the method's generalization. By providing a scale-independent measurement, the relative MAD is not affected by the absolute range of temperatures, allowing for comparisons across various regions or time periods, including different seasons or climatic contexts. The relative MAD, along with the indicators dEF_{dry} and dEF_{wet} plays complementary roles in addressing the method's assumptions. While relative MAD confirms the method's feasibility, ensuring that at least one of the EF method groups works, the derivative values help to discard ineffective methods. This two-step approach enhances the robustness of the overall methodology, providing both reliability and applicability across different climatic and environmental conditions.

However, the use of these indicators includes the definition of thresholds to manage heterogeneity levels or identify situations. This means that the method is mainly dependent on the efficiency of the thresholds. In this study, the thresholds were calibrated on a single flux measurement site, in an area characterized by a high level of land cover heterogeneity and also by pronounced seasonal pattern. Results show that seasonality is successfully reproduced based on a good recognition of different situations. Nevertheless, since the method relies on threshold determination, it is never completely free from threshold effects, i.e., thresholds act as a tipping point mainly in transition periods, which can sometimes lead to confusion in the situation's identification. Indeed, some confusions are observed, mainly between the wet and transition periods or between the transition and dry periods (see Fig. 9). However, as shown in Fig. 9, the number of days with confusion is very small compared to the total number of days in the corresponding season. Furthermore, if confusion occurs between two situations, it means that they produce fairly similar estimates, so the impact on evapotranspiration estimation is not that significant. The efficiency of the method is thus much greater than the confusions it causes. Nevertheless, the defined thresholds may not be applicable across all areas. Therefore, a calibration phase is required, especially if the method is applied in a study area with different climatic and heterogeneity characteristics. For fine local scale applications, thresholds should be recalibrated according to the eco-climatic zone. However, for a global application, a more refined strategy may be needed to estimate generalized thresholds on a larger geographic scale. Generalized thresholds should then be calibrated using a large set of flux towers (i.e., Fluxnet).

However, this generalization may come at the expense of ET estimation accuracy on specific sites.

The use of high thermal spatial resolution data in our study area will enable better surface heterogeneity estimation, which will help detect more thermal contrast in the image. In this case, the threshold defined for dispersion assessment, set at 2 for this study, could remain the same, as the relative MAD, as explained above, is not influenced by the absolute temperature range. It is only expected that relative MAD should be less frequently lower than the threshold. Secondly, dry and wet edges can be more easily identified when using satellite data with higher spatial resolution. The different EF estimation methods will likely produce very similar results, making method selection less significant in this case. For this reason, contextual methods are known to be more adapted with high spatial resolution data.

While the EF methods' selection algorithm proposed in this study appears to be very relevant with the S-SEBI contextual model, it also seems promising to improve other contextual models, such as the LST-VI triangle methods. Adapting the selection algorithm to these triangle methods will probably need a recalibration of the selection thresholds, particularly on dEF_{dry} and dEF_{wet} . It would then allow for a reduction of the structural uncertainty in ensemble contextual methods, such as the full EVASPA tool (Gallego-Elvira et al., 2013), and bring more robust ET estimations in almost every climatic conditions. Indeed, EF method selection represents the major source of uncertainty in all contextual methods (Olioso et al., 2023; Mwangi et al., 2024). Nevertheless, uncertainties are also induced by the inputs used to constrain the model. Olioso et al. (2023), Mwangi et al. (2024) show that contextual models are very sensitive to the global radiation and atmospheric radiation used for Rn and subsurface soil heat flux (G) estimation. The Rn and G components are computed independently from EF estimation. Therefore, accumulated uncertainties from these different variables (Rn, G and EF) could produce additional errors. The analysis performed in this work is impacted by missing information during the whole wet season. Indeed, satellite acquisition is constrained by the presence of clouds. This represents a limiting factor in our study area, which is characterized by a strong seasonal climatic contrast, with the alternation of a dry season and a monsoon period. In other semi-arid climatic contexts, this problem could be less important since the rainy season is shorter and irregular (Allies et al., 2020). To derive seasonal evapotranspiration, the gaps between satellite acquisitions need to be filled in order to reconstruct days with missing ET data (Allies et al., 2022; Delogu et al., 2021).

5. Conclusions

The present study introduces an innovative approach for the automatic selection of adapted methods for EF estimation using an ensemble contextual energy balance model called E3S (Allies et al., 2020). The latter relies on a heterogeneity assumption in order to compute reliable EF estimates, and therefore, it relies on an accurate estimation of evapotranspiration rates. In Allies et al. (2020), EF estimation involves a solid understanding of the study area in order to select an appropriate method to use according to the season. This study proposes generalizing and facilitating the application of the approach proposed in Allies et al. (2020) by using a heterogeneity assessment based only on image information. The derivative of the EF with respect to LST_{dry} and the derivative of the EF with respect to LST_{wet} , denoted " dEF_{dry} " and "dEFwet", respectively, were calculated to identify the positioning of $LST - \alpha$ regarding the wet and dry edges. Consequently, adapted methods for each situation could be identified independently from seasonal or any other additional information. The proposed method succeeded in reducing the structural uncertainties related to EF method selection significantly. Hence, it tackled the major source of errors in contextual methods. These latter are selected to be used for TRISHNA mission (CNES/ISRO) (Lagouarde et al., 2018) ET estimation, since they use a reduced number of inputs and have fewer uncertainty sources than

single pixel methods. E3S-V2 method could be also a good candidate algorithm for TRISHNA ET product.

E3S-V2 method was evaluated in this work using kilometric satellite data from MODIS. Although the resolution might be too low to provide sufficient thermal contrast in specific conditions, MODIS high temporal resolution is very useful for the method implementation and evaluation. Thermal information from higher-resolution data is expected to further improve ET simulation by capturing more heterogeneity in satellite images. Upcoming thermal Earth observation missions like TRISHNA, LSTM (ESA, Koetz et al. (2019)) or SBG (NASA, Cawse-Nicholson et al. (2021)) could lead to more accurate estimates of the surface water deficit in semi-arid areas using this method.

CRediT authorship contribution statement

Nesrine Farhani: Writing - original draft, Visualization, Software, Methodology, Investigation, Formal analysis, Data curation, Conceptualization. Jordi Etchanchu: Visualization, Validation, Supervision, Software, Methodology, Data curation, Conceptualization. Gilles Boulet: Project administration, Funding acquisition, Conceptualization. Philippe Gamet: Visualization, Project administration. Albert Olioso: Visualization, Validation, Conceptualization. Alain Dezetter: Software, Resources. Ansoumana Bodian: Data curation. Nanée Chahinian: Visualization, Resources. Kanishka Mallick: Visualization, Conceptualization, Chloé Ollivier: Visualization, Data curation. Olivier Roupsard: Formal analysis, Data curation. Aubin Allies: Methodology. Jérôme Demarty: Visualization, Validation, Supervision, Investigation, Funding acquisition, Conceptualization.

Declaration of competing interest

The authors declare the following financial interests/personal relationships which may be considered as potential competing interests: The authors declare that:

- · The work described has not been published previously except in the form of a preprint, an abstract, a published lecture, academic thesis or registered report,
- the article is not under consideration for publication elsewhere.
- · the article's publication is approved by all authors and tacitly or explicitly by the responsible authorities where the work was carried out.
- · if accepted, the article will not be published elsewhere in the same form, in English or in any other language, including electronically without the written consent of the copyright-holder.

Acknowledgments

The authors gratefully acknowledge financial support by French Space Agency (CNES) in the frame of the preparation of the TRISHNA mission and the UNESCO Centre for Water ICIREWARD through the EVAP'EAU project in which the present work has been realized. We would also wish to thank the EcoSols laboratory and the IESOL mixed international laboratory for their help in understanding the area's hydrometeorological behavior and for sharing the Niakhar Faidherbia-flux data.

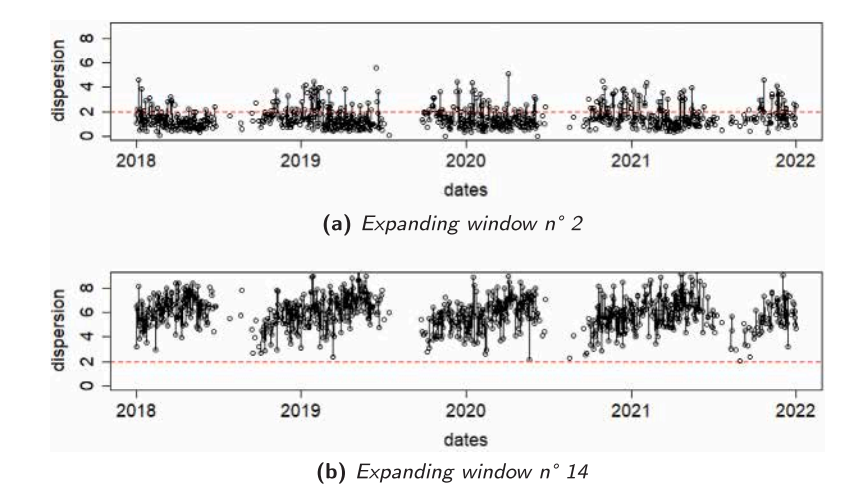


Fig. 15. Temporal variation of the dispersion coefficient calculated from expanding windows 2 and 14.

Appendix A. Method evaluation

A.1. Data for comparison

In order to evaluate "E3S-V2", in-situ measurements and spatially distributed variables other than inputs are also used for this purpose.

- In-situ measurements: Niakhar station (14.4958°N, 16.4536°W), installed in 2018 by the IESOL Mixed International Laboratory (Roupsard et al., 2020), provides half-hourly observations of the climate evolution. The flux site provides observations on a typical cropland under acacia trees (Faidherbia albida). The instrumentation includes two eddy-covariance measurements at different heights (at 4.5 m and 20 m), in order to monitor the entire agroforestery plot and the underlying crop only. This gauging station estimates the energy and carbon turbulent fluxes using a LI-COR LI-7500 gas analyzer combined with a GILL WindMaster 3D sonic anemometer. Convective fluxes exchanged between the surface and the atmosphere, the net radiation and the soil heat flux are collected using different instruments at different levels and used as the ground truth for the assessment of the E3S-V2 simulations. For comparison purposes, we have computed daily ET estimation from gap-filled LE measurements provided initially at sub-daily scale. The gap-filling is performed using the REddyProc R package (Wutzler et al., 2018). This method is based on relating meteorological variables to ET on available periods in order to define different meteorological classes. These latter are then used to gap-fill ET series with the corresponding ET mean.
- ET product from the GLEAM dataset: The global ET product from the Global Land Evaporation Amsterdam Model (GLEAM) (Miralles et al., 2011), developed by the VU University of Amsterdam, is available at a daily scale and at 0.25° of spatial resolution, and it is used in our work for mesoscale comparison with ET E3S-V2 simulations. Indeed, the GLEAM product has been deemed a good reference for the African continent and in the Sahel region (Trambauer et al., 2014). Moreover, in Etchanchu et al. (2025), this product showed the best performance in comparison with other available daily RS-ET products in semi-arid African areas and at the regional scale. GLEAM products use a range of independent remotely sensed observations to estimate daily actual evapotranspiration based on the Priestley and Taylor (PT) evaporation formula in combination with an evaporative stress module derived from soil moisture (Moctar et al., 2020) and the Gash analytical model of rainfall interception (Miralles et al., 2011) in order to derive actual evaporation.

- ET product from ERA5-Land: The ET product provided by ERA5-Land was also used for a mesoscale comparison with E3S-V2 simulations, since it showed a high performance in our study area according to Etchanchu et al. (2025). Similarly to the meteorological products, the ET product is available at a 9 km spatial resolution and at a daily temporal scale. ET is computed using atmospheric forcing data from ERA5 and soil and vegetation parameters (Muñoz-Sabater et al., 2021) in order to solve the energy-water balance along a soil-plant-atmosphere interface with the H-TESSEL model (Balsamo et al., 2009).
- LAI data: We used the four-day LAI from the Combined MODIS data (MCD15A3). This variable is used to simulate the initial E3S version as a dynamic weighting scheme of ET estimates derived from several EF methods.

A.2. Daily ET from instantaneous latent heat flux

For more interpretable hydrological estimates, "E3S-V2" method is evaluated and compared to other ET products, using daily ET estimates rather than instantaneous estimates. Daily ET estimates are extrapolated from instantaneous estimations (LE) to reconstruct hourly variations using global radiation (Rg) data. Indeed, ET is assumed to follow the same diurnal variation as the incoming global solar radiation (Rg) on clear days (Delogu et al., 2012). Then, based on the "self-preservation" hypothesis, which assumes that the ratio LE/Rg remains fairly constant during daytime (Lhomme and Elguero, 1999; Delogu et al., 2012), daily ET can be simply derived from the daily ETd/Rgd ratio and the instantaneous estimate of LE and Rg at the time of the satellite overpass (see Eq. (8)).

$$ET_d = \frac{1}{\lambda} Rg_d * \frac{LE}{Rg_t},\tag{8}$$

where ET_d is the daily evapotranspiration, usually expressed in mm d^{-1} , and Rg_d is the cumulative daily global incoming solar radiation. The LE and Rg_t are estimates of these components at the time of the satellite overpass (t), and λ is the latent heat.

A.3. Data aggregation

An up-scaling (data aggregation) procedure is needed to fill the scale gap between the simulations from MODIS (E3S-V2) and the other gridded products used for comparison. ET data from GLEAM and ERA5-Land, which are available at a lower spatial resolution, can then be compared to up-scaled (aggregated) simulations derived from MODIS products, available initially at the kilometric scale. A simple averaging approach is used for this work; it is often used for data aggregation

Table 3
Methods of LST-albedo edge determination in E3S

Method name	Domain division	Dry edge calculation	Wet edge calculation	Method type	Reference
EF1	20 intervals of same pixel density	Linear regression obtained from points corresponding to the median of the 5% highest LST values for each interval	Linear regression obtained from points corresponding to the median of the 5% highest LST values for each interval	"Mixed method"	Gallego-Elvira et al. (2013)
EF8			LST_{min}	"Dry method"	
EF12		LST_{max}	EF1	"Wet method"	
EF2	Removal of LST values with lowest probability distribution. LST-albedo domain is divided into 20 intervals of the same pixel density	Linear regression obtained from points corresponding to the maximum LST value and albedo median for each interval	Linear regression obtained from points corresponding to the minimum LST value and albedo median for each interval	"Mixed method"	Gallego-Elvira et al. (2013), adapted from Tang et al. (2010)
EF9 EF13		LST_{max}	LST_{min}	"Dry method" "Wet method"	
EF4	N intervals of 0.05 albedo value between 0.05 and the first multiple greater than the observed maximum albedo value	Linear regression obtained from points corresponding to an exceedance frequency of 97.5% of LST values and albedo median	Linear regression obtained from points corresponding to an exceedance frequency of 2.5% of LST values and albedo median	"Mixed method"	Gallego-Elvira et al. (2013)
EF10 EF16		LST_{max}	LST_{min} EF4	"Dry method" "Wet method"	
EF7	N intervals of 0.05 albedo value between 0.05 and the first multiple greater than the observed maximum albedo value	Second-order polynomial obtained from points corresponding to an exceedance frequency of 97.5% of LST values and albedo median	Second-order polynomial obtained from points corresponding to an exceedance frequency of 2.5% of LST values and albedo median	"Mixed method"	Gallego-Elvira et al. (2013)
EF11 EF14		LST_{max}	LST_{min} EF7	"Dry method" "Wet method"	
Split	N intervals of 0.01 albedo value between the minimum and maximum albedo values in the image	Linear regression obtained from points corresponding to the median of 5% unique maximum LST values and albedo median	Linear regression obtained from points corresponding to the median of 5% unique maximum LST values and albedo median	"Mixed method"	Verstraeten et al. (2005)
EF17 EF20		LST_{max}	<i>LST_{min}</i> Split	"Dry method" "Wet method"	
Inflex	Split	Linear regression obtained from N points $(\alpha > \alpha_i)$ corresponding to the median of 5% unique maximum LST values and albedo median. A horizontal line defined by the LST_{max} value completes the left part of the dry edge for pixels with $\alpha < \alpha_i$	Linear regression obtained from points corresponding to the median of 5% unique maximum LST values and albedo median	"Mixed method"	Adapted from Verstraeten et al. (2005)
EF19 EF18		Linear regression obtained from points corresponding to the median of the 5% highest LST values for each interval	LST_{min} LST_{min}	"Dry method" "Dry method"	

schemes, since it preserves the mean value of the original image and provides a better representation of the initial data values (Hong et al., 2009; Sharma et al., 2016).

Appendix B. Method implementation

B.1. Dispersion coefficient validation

To validate the already defined dispersion coefficient in Section 3.1, the temporal variations of this coefficient estimated using sub-area 2 and the whole study area (sub-area 14) during the study period are compared (Fig. 15). Using sub-area 2, the dispersion is almost always lower than 2, which means that there is insufficient dispersion for the LST values observed in the utilized area. However, when using the whole study area, which is characterized by sufficiently heterogeneous conditions, the dispersion coefficient is always above the threshold defined for dispersion assessment.

B.2. Thresholds estimation

The analysis of the temporal variability of dEF values validate the thresholds identified in Section 3.2. Figs. 16(a) and 16(b) represent 50% of dEF_{dry} and dEF_{wet} , corresponding to the thresholds identified above, using only the adapted methods for the dry and wet seasons. Indeed, as observed above in Fig. 8, the median value of dEF is very representative of dEF's overall distribution, and using it will filter out values with a very low frequency that could induce incorrect interpretations. Fig. 16(a) shows that by using adapted methods for the dry season, the dry season can be correctly identified. This is also true for the wet season.

Data availability

Data will be made available on request.

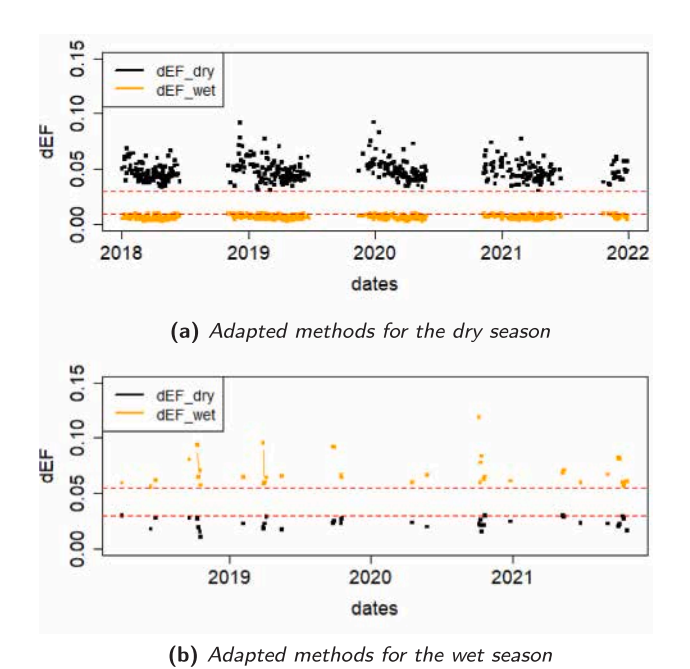


Fig. 16. Temporal variability of the medians of dEF_{drv} and dEF_{wet} over the study

period (2018–2022) using adapted methods for the dry and wet seasons.

References

- Allen, R., Tasumi, M., Trezza, R., 2007. Satellite-based energy balance for mapping evapotranspiration with internalized calibration (METRIC)—Model. J. Irrig. Drain. Eng. 133 (4), 380–394.
- Allies, A., Demarty, J., Olioso, A., Bouzou M, I., Issoufou, H.B., Velluet, C., Bahir, M., Maïnassara, I., Oï, M., Chazarin, J.-P., et al., 2020. Evapotranspiration estimation in the sahel using a new ensemble-contextual method. Remote. Sens. 12 (3), 380.
- Allies, A., Olioso, A., Cappelaere, B., Boulet, G., Etchanchu, J., Barral, H., Moussa, I., Chazarin, J.-P., Delogu, E., Issoufou, H., et al., 2022. A remote sensing data fusion method for continuous daily evapotranspiration mapping at kilometric scale in sahelian areas. J. Hydrol. 607, 127504.
- Anderson, M., Kustas, W., 2008. Thermal remote sensing of drought and evapotranspiration. Eos, Trans. Am. Geophys. Union 89 (26), 233–234.
- Arachchige, C.N., Prendergast, L.A., Staudte, R.G., 2022. Robust analogs to the coefficient of variation. J. Appl. Stat. 49 (2), 268–290.
- Balsamo, G., Beljaars, A., Scipal, K., Viterbo, P., van den Hurk, B., Hirschi, M., Betts, A., 2009. A revised hydrology for the ECMWF model: Verification from field site to terrestrial water storage and impact in the integrated forecast system. J. Hydrometeorol. 10 (3), 623–643.
- Bastiaanssen, W.G., Menenti, M., Feddes, R., Holtslag, A., 1998. A remote sensing surface energy balance algorithm for land (SEBAL). 1. formulation. J. Hydrol. 212, 198–212.
- Boulet, G., Chehbouni, A., Gentine, P., Duchemin, B., Ezzahar, J., Hadria, R., 2007.
 Monitoring water stress using time series of observed to unstressed surface temperature difference. Agricult. Forest. Meterol. 146 (3–4), 159–172.
- Boulet, G., Mougenot, B., Lhomme, J.-P., Fanise, P., Lili-Chabaane, Z., Olioso, A., Bahir, M., Rivalland, V., Jarlan, L., Merlin, O., et al., 2015. The SPARSE model for the prediction of water stress and evapotranspiration components from thermal infra-red data and its evaluation over irrigated and rainfed wheat. Hydrol. Earth Syst. Sci. 19 (11), 4653–4672.
- Carlson, T., 2007. An overview of the "triangle method" for estimating surface evapotranspiration and soil moisture from satellite imagery. Sensors 7 (8), 1612–1629.
- Carlson, T.N., Gillies, R.R., Schmugge, T.J., 1995. An interpretation of methodologies for indirect measurement of soil water content. Agricult. Forest. Meterol. 77 (3–4), 191–205.
- Carlson, T.N., Petropoulos, G.P., 2019. A new method for estimating of evapotranspiration and surface soil moisture from optical and thermal infrared measurements: The simplified triangle. Int. J. Remote Sens. 40 (20), 7716–7729.
- Cawse-Nicholson, K., Townsend, P.A., Schimel, D., Assiri, A.M., Blake, P.L., Buongiorno, M.F., Campbell, P., Carmon, N., Casey, K.A., Correa-Pabón, R.E., et al., 2021. Nasa's surface biology and geology designated observable: A perspective on surface imaging algorithms. Remote Sens. Environ. 257, 112349.

- Chehbouni, A., Escadafal, R., Duchemin, B., Boulet, G., Simonneaux, V., Dedieu, G., Mougenot, B., Khabba, S., Kharrou, H., Maisongrande, P., et al., 2008. An integrated modelling and remote sensing approach for hydrological study in arid and semi-arid regions: The SUDMED programme. Int. J. Remote Sens. 29 (17–18), 5161–5181.
- Chen, J.M., Liu, J., 2020. Evolution of evapotranspiration models using thermal and shortwave remote sensing data. Remote Sens. Environ. 237, 111594.
- Chirouze, J., Boulet, G., Jarlan, L., Fieuzal, R., Rodriguez, J., Ezzahar, J., Er-Raki, S., Bigeard, G., Merlin, O., Garatuza-Payan, J., et al., 2014. Intercomparison of four remote-sensing-based energy balance methods to retrieve surface evapotranspiration and water stress of irrigated fields in semi-arid climate. Hydrol. Earth Syst. Sci. 18 (3), 1165–1188.
- Delogu, E., Boulet, G., Olioso, A., Coudert, B., Chirouze, J., Ceschia, E., Le Dantec, V., Marloie, O., Chehbouni, G., Lagouarde, J.-P., 2012. Reconstruction of temporal variations of evapotranspiration using instantaneous estimates at the time of satellite overpass. Hydrol. Earth Syst. Sci. 16 (8), 2995–3010.
- Delogu, E., Olioso, A., Alliès, A., Demarty, J., Boulet, G., 2021. Evaluation of multiple methods for the production of continuous evapotranspiration estimates from TIR remote sensing. Remote. Sens. 13 (6), 1086.
- Ershadi, A., McCabe, M., Evans, J.P., Chaney, N.W., Wood, E.F., 2014. Multi-site evaluation of terrestrial evaporation models using fluxnet data. Agricult. Forest. Meterol. 187, 46–61.
- Etchanchu, J., Demarty, J., Dezetter, A., Farhani, N., Thiam, P.B., Allies, A., Bodian, A., Boulet, G., Chahinian, N., Diop, L., et al., 2025. Multiscale analysis of existing actual evapotranspiration products over agropastoral sahel. J. Hydrol. 651, 132585.
- Gallego-Elvira, B., Olioso, A., Mira, M., Reyes-Castillo, S., Boulet, G., Marloie, O., Garrigues, S., Courault, D., Weiss, M., Chauvelon, P., et al., 2013. EVASPA (evapotranspiration assessment from space) tool: An overview. Procedia Environ. Sci. 19, 303–310.
- Hong, S., Hendrickx, J.M., Borchers, B., 2009. Up-scaling of SEBAL derived evapotranspiration maps from landsat (30 m) to MODIS (250 m) scale. J. Hydrol. 370 (1–4), 122–138.
- Jiang, L., Islam, S., 1999. A methodology for estimation of surface evapotranspiration over large areas using remote sensing observations. Geophys. Res. Lett. 26 (17), 2773–2776.
- Jiang, L., Islam, S., 2001. Estimation of surface evaporation map over southern great plains using remote sensing data. Water Resour. Res. 37 (2), 329–340.
- Jiang, L., Islam, S., 2003. An intercomparison of regional latent heat flux estimation using remote sensing data. Int. J. Remote Sens. 24 (11), 2221–2236.
- Kizito, F., Dragila, M., Sene, M., Lufafa, A., Diedhiou, I., Dick, R., Selker, J., Dossa, E., Khouma, M., Badiane, A., et al., 2006. Seasonal soil water variation and root patterns between two semi-arid shrubs co-existing with pearl millet in Senegal, west africa. J. Arid. Environ. 67 (3), 436–455.
- Koetz, B., Berger, M., Blommaert, J., Del Bello, U., Drusch, M., Duca, R., Gascon, F., Ghent, D., Hoogeveen, J., Hook, S., et al., 2019. Copernicus High Spatio-Temporal Resolution Land Surface Temperature Mission: Mission Requirements Document. ESA, Noordwijk, The Netherlands.
- Kustas, W.P., Norman, J., 1999. Evaluation of soil and vegetation heat flux predictions using a simple two-source model with radiometric temperatures for partial canopy cover. Agricult. Forest. Meterol. 94 (1), 13–29.
- Lagouarde, J.-P., Bhattacharya, B., Crebassol, P., Gamet, P., Babu, S., Boulet, G., Briottet, X., Buddhiraju, K., Cherchali, S., Dadou, I., et al., 2018. The Indian-french trishna mission: Earth observation in the thermal infrared with high spatio-temporal resolution. In: IGARSS 2018-2018 IEEE International Geoscience and Remote Sensing Symposium. IEEE, pp. 4078–4081.
- Lagouarde, J.P., Boulet, G., 2016. Energy balance of continental surfaces and the use of surface temperature. In: Land Surface Remote Sensing in Continental Hydrology. Elsevier, pp. 323–361.
- Lhomme, J.-P., Elguero, E., 1999. Examination of evaporative fraction diurnal behaviour using a soil-vegetation model coupled with a mixed-layer model. Hydrol. Earth Syst. Sci. 3 (2), 259–270.
- Liang, S., Rui, S., Xiaowen, L., Huailiang, C., Xuefen, Z., 2011. Estimating evapotranspiration using improved fractional vegetation cover and land surface temperature space. J. Resour. Ecol. 2 (3), 225–231.
- Long, D., Singh, V.P., 2013. Assessing the impact of end-member selection on the accuracy of satellite-based spatial variability models for actual evapotranspiration estimation. Water Resour. Res. 49 (5), 2601–2618.
- Miralles, D., De Jeu, R., Gash, J., Holmes, T., Dolman, A., 2011. Magnitude and variability of land evaporation and its components at the global scale. Hydrol. Earth Syst. Sci. 15 (3), 967–981.
- Moctar, D., Natalie, C., JZ, S., S, E., M, G., S, B., 2020. Potential of satellite and reanalysis evaporation datasets for hydrological modelling under various model calibration strategies. Adv. Water Resour. 143, 103667. http://dx.doi.org/10.1016/ j.advwatres.2020.103667, URL: https://www.sciencedirect.com/science/article/pii/ S030917082030230X.
- Mueller, B., Hirschi, M., Jimenez, C., Ciais, P., Dirmeyer, P.A., Dolman, A.J., Fisher, J.B., Jung, M., Ludwig, F., Maignan, F., et al., 2013. Benchmark products for land evapotranspiration: LandFlux-eval multi-data set synthesis. Hydrol. Earth Syst. Sci. 17 (10), 3707–3720.

- Muñoz-Sabater, J., Dutra, E., Agustí-Panareda, A., Albergel, C., Arduini, G., Balsamo, G., Boussetta, S., Choulga, M., Harrigan, S., Hersbach, H., et al., 2021. ERA5-land: A state-of-the-art global reanalysis dataset for land applications. Earth Syst. Sci. Data 13 (9), 4349–4383.
- Mwangi, S., Olioso, A., Boulet, G., Farhani, N., Etchanchu, J., Demarty, J., Ollivier, C., Hu, T., Mallick, K., Jia, A., et al., 2024. Ensemble estimation of evapotranspiration using EVASPA: a multi-data multi-method analysis. In: IGARSS 2024-2024 IEEE International Geoscience and Remote Sensing Symposium. IEEE, pp. 2475–2478.
- Norman, J., Kustas, W., Humes, K., 1995. Source approach for estimating soil and vegetation energy fluxes in observations of directional radiometric surface temperature. Agricult. Forest. Meterol. 77 (3–4), 263–293.
- Norton, M.R., Malinowski, D.P., Volaire, F., 2016. Plant drought survival under climate change and strategies to improve perennial grasses. a review. Agron. Sustain. Dev. 36. 1–15.
- Olioso, A., Carrière, S., Allies, A., Desrutins, H., Sobrino, J., Skoković, D., Demarty, J., Boulet, G., Weiss, M., Buis, S., 2023. Evapotranspiration mapping from remote sensing data: Uncertainties and ensemble estimates based on multimodel–multidata simulations. In: Proc. Int. Workshop High-Resolution Thermal EO. p. 1.
- Olioso, A., Gallego-Elvira, B., Bahir, M., Boulet, G., Weiss, M., Sarrio, M., Castillo, S., 2015. EVASPA: Evapotranspiration assessment from space. In: Workshop Modélisation De Surface.
- Panthou, G., Lebel, T., Vischel, T., Quantin, G., Sane, Y., Ba, A., Ndiaye, O., Diongue-Niang, A., Diopkane, M., 2018. Rainfall intensification in tropical semi-arid regions: The sahelian case. Environ. Res. Lett. 13 (6), 064013.
- Ragab, R., Prudhomme, C., 2002. Sw—soil and water: Climate change and water resources management in arid and semi-arid regions: Prospective and challenges for the 21st century. Biosyst. Eng. 81 (1), 3–34.
- Roerink, G., Su, Z., Menenti, M., 2000. S-SEBI: A simple remote sensing algorithm to estimate the surface energy balance. Phys. Chem. the Earth, Part B: Hydrol. Ocean. Atmosphere 25 (2), 147–157.
- Roupsard, O., Audebert, A., Ndour, A., Clermont-Dauphin, C., Agbohessou, Y., Sanou, J., Koala, J., Faye, E., Sambakhe, D., Jourdan, C., et al., 2020. How far does the tree affect the crop in agroforestry? New spatial analysis methods in a faidherbia parkland. Agric. Ecosyst. Environ. 296, 106928.

- Sharma, V., Kilic, A., Irmak, S., 2016. Impact of scale/resolution on evapotranspiration from landsat and modis images. Water Resour. Res. 52 (3), 1800–1819.
- Sheffield, J., Wood, E.F., 2012. Drought: Past Problems and Future Scenarios. Routledge.
- Su, Z., 2002. The surface energy balance system (SEBS) for estimation of turbulent heat fluxes. Hydrol. Earth Syst. Sci. 6 (1), 85–100.
- Tang, R., Li, Z.-L., 2017. An improved constant evaporative fraction method for estimating daily evapotranspiration from remotely sensed instantaneous observations. Geophys. Res. Lett. 44 (5), 2319–2326.
- Tang, R., Li, Z.-L., Tang, B., 2010. An application of the ts-VI triangle method with enhanced edges determination for evapotranspiration estimation from MODIS data in arid and semi-arid regions: Implementation and validation. Remote Sens. Environ. 114 (3), 540–551.
- Trambauer, P., Dutra, E., Maskey, S., Werner, M., Pappenberger, F., Van Beek, L., Uhlenbrook, S., 2014. Comparison of different evaporation estimates over the african continent. Hydrol. Earth Syst. Sci. 18 (1), 193–212.
- Trenberth, K., 2011. Changes in precipitation with climate change. Clim. Res. 47 (1–2), 123–138.
- Verstraeten, W.W., Veroustraete, F., Feyen, J., 2005. Estimating evapotranspiration of European forests from NOAA-imagery at satellite overpass time: Towards an operational processing chain for integrated optical and thermal sensor data products. Remote Sens. Environ. 96 (2), 256–276.
- Vogt, J., Naumann, G., Masante, D., Spinoni, J., Cammalleri, C., Erian, W., Pischke, F., Pulwarty, R., Marinho Ferreira Barbosa, P., 2018. Drought risk assessment and management: A conceptual framework. EUR 29464 EN, Publications Office of the European Union, Luxembourg, ISBN: 978-92-79-97470-0, http://dx.doi.org/10. 2760/919458.JRC113937.
- Wutzler, T., Reichstein, M., Moffat, A., Migliavacca, M., 2018. REddyProc: Post processing of (half-) hourly eddy-covariance measurements, r package version 1.2.
- Zhang, R., Tian, J., Su, H., Sun, X., Chen, S., Xia, J., 2008. Two improvements of an operational two-layer model for terrestrial surface heat flux retrieval. Sensors 8 (10), 6165–6187.
- Zhu, W., Jia, S., Lall, U., Cheng, Y., Gentine, P., 2020. An observation-driven optimization method for continuous estimation of evaporative fraction over large heterogeneous areas. Remote Sens. Environ. 247, 111887.